POLITECNICO DI TORINO
Repository ISTITUZIONALE

Multilayered plate elements accounting for refined theories and node-dependent kinematics

(Article begins on next page)

17 July 2024

Multilayered plate elements accounting for refined theories and node-dependent kinematics

E. Carrera, A. Pagani, S. Valvano

Mul^2 Group, Department of Mechanical and Aerospace Engineering
Politecnico di Torino, Turin, Italy

Keywords:
Multilayered plate elements, Refined theories, Global/local analysis, Carrera unified formulation, Node-dependent kinematics.

Author and address for Correspondence
Dr. Erasmo Carrera
Professor of Aerospace Structures and Aeroelasticity,
Department of Mechanical and Aerospace Engineering
Politecnico di Torino,
Corso Duca degli Abruzzi, 24,
10129 Torino, ITALY,
tel +39.011.546.6836, fax +39.011.564.6899
e.mail: erasmo.carrera@polito.it

Abstract

In the present work, a new class of finite elements (FEs) for the analysis of metallic and composite plates is proposed. By making use of node-by-node variable plate theory assumptions, the new finite element allows for the simultaneous analysis of different subregions of the problem domain with different kinematics and accuracy, in a global/local sense. As a consequence, the computational costs can be reduced drastically by assuming refined theories only in those zones/nodes of the structural domain where the resulting strain and stress states present a complex distribution. On the contrary, computationally cheaper, low-order kinematic assumptions can be used in the remaining parts of the plate where a localized detailed analysis is not necessary. The primary advantage of the present variable-kinematics element and related global/local approach is that no ad-hoc techniques and mathematical artifices are required to mix the fields coming from two different and kinematically incompatible adjacent elements, because the plate structural theory varies within the finite element itself. In other words, the structural theory of the plate element is a property of the FE node in this present approach, and the continuity between two adjacent elements is ensured by adopting the same kinematics at the interface nodes. In this paper, the novel variable-kinematics plate element is implemented by utilizing the Carrera Unified Formulation (CUF), whose main advantage consists in the possibility of keeping the order of the expansion of the state variables along the thickness of the plate as a free parameter of the model. According to CUF, Taylor polynomial expansions are used to describe the through-the-thickness unknowns to develop classical to higher-order Equivalent Single Layer (ESL) plate theories. Furthermore, the Mixed Interpolated Tensorial Components (MITC) method is employed to contrast the shear locking phenomenon. Several numerical investigations are carried out to validate and demonstrate the accuracy and efficiency of the present plate element, including comparison with various closed-form and FE solutions from the literature.

1 Introduction

Plate structures have a predominant role in a variety of engineering applications. Nevertheless, the use of new materials, such as composites layered materials, leads to increasingly complex structural designs that require careful and detailed analysis. The analysis of layered composite structures is complicated in practice. In some cases, structures may contain regions where three-dimensional (3D) stress fields occur. To accurately capture these localized 3D stress states, solid models or higher-order theories are necessary. However, the high computational costs represent the drawback of refined plate theories or three-dimensional analyses.

The Finite Element Method (FEM) has a predominant role among the computational techniques implemented for the analysis of layered structures. The majority of FEM theories available in the literature are formulated by axiomatic-type theories. The conventional FEM plate model is the classical Kirchhoff-Love theory, and some examples are given in [1, 2], whose extension to laminates is known to as the Classical Lamination Theory (CLT) [3]. Another classical plate element is based on the First-order Shear Deformation Theory (FSDT), which rely on the works by Reissner [4] and Mindlin [5]. To overcome the limitations of classical theories, a large variety of plate finite element implementations of higher-order theories (HOT) have been proposed in the last years. HOT-based C^0 finite elements (C^0 means that the continuity is required only for the unknown variables and not for their derivatives) were discussed by Kant *et al.* [6] and Kant and Kommineni [7]. Many other papers are available in which HOTs have been implemented for plates, and more details can be found in the books from Reddy [8] and Palazzotto and Dennis [9].

Although the enormous improvements and formulations of higher-order plate structural theories, considerable work has been recently directed towards the implementation of innovative solutions for

improving the analysis efficiency for complex geometries and assemblies, possibly in a global/local scenario. In this manner, the limited computational resources can be distributed in an optimal manner to study in detail only those parts of the structure that require an accurate analysis. In general, two main approaches are available to deal with a global/local analysis: (1) refining the mesh or the FE shape functions in correspondence with the critical domain; (2) formulating multi-model methods, in which different subregions of the structure are analysed with different mathematical models. To couple coarse and refined mesh discretizations of different subregions of a structure, adaptive techniques are often used. The h-adaption method [10] is used when the structures subregions differ in mesh size, whereas the p-adaption method [11] can be applied when the subregions vary in the polynomial order of the shape functions. Moreover, the hp-adaption [12] can allow the implementation of subregions differing in both mesh size and shape functions. The methods mentioned so far can be addressed as single-theory or single-model methods.

In the case of multi-theory methods, in which different subregions of the structure are analysed with different structural theories with kinematically incompatible elements, the compatibility of displacements and equilibrium of stresses at the interface between dissimilar elements have to be achieved. A wide variety of multiple model methods have been reported in the literature. In general, multi-theory methods can be divided into sequential or multistep methods, and simultaneous methods. In a sequential multi-model, the global region is analysed with an adequate model with a cheap computational cost to determine the displacement or force boundary conditions for a subsequent analysis at the local level. The local region can be modeled with a more refined theory, or it can be modeled with 3-D finite elements, see [13, 14, 15, 16]. The simultaneous multi-model methods are characterized by the analysis of the entire structural domain, where different subregions are modeled with different mathematical models and/or distinctly different levels of domain discretization, in a unique step. One of the simplest type of simultaneous multi-model methods for composite laminates analysis, is the concept of selective ply grouping or sublaminates [17, 18, 19]. In the literature, the local region (i.e., the region where accurate stress analysis is desired) is generally modeled by using 3-D finite elements in the domain of selective ply grouping method. Recently, the authors developed multi-model elements with variable through-the-thickness approximation by using 2-D finite elements for both local and global regions [20]. In this approach, the continuity of the primary variables between local and global regions was straightforwardly satisfied by employing Legendre polynomials. In the work by Botshekanan Dehkordi *et al.* [21], a variable description in the thickness direction for the static analysis of sandwich plates was performed. That model was derived from the Reisnner-Mixed-Variational-Theorem (RMVT) in order to describe a-priori the transverse shear and normal stresses. The same mixed approach was then used in [22] for the nonlinear dynamic analysis of sandwich plates with flexible core and composite faces embedded with shape memory alloy wires. Another well-known method to couple incompatible kinematics in multi-model methods, is the use of Lagrange multipliers, which serve as additional equations to enforce compatibility between adjacent subregions. In the three-field formulation by Brezzi and Marini [23], an additional grid at the interface is introduced. The unknowns are represented independently in each sub-domain and at the interface, where the matching is provided by suitable Lagrange multipliers. This method was recently adopted by Carrera et al. [24, 25, 26] to couple beam elements of different orders and, thus, to develop variable kinematic beam theories. Ben Dhia *et al.* [27, 28, 29, 30] proposed the Arlequin method to couple different numerical models by means of a minimization procedure. This method was adopted by Hu *et al.* [31, 32] for the linear and non-linear analysis of sandwich beams modelled via one-dimensional and two-dimensional finite elements, and by Biscani *et al.* [33] for the analysis of beams and by Biscani *et al.* [34] for the analysis of plates. Reddy and Robbins [35] and Reddy [36] presented a multiple-model method on the basis of a variable kinematic theory and on mesh superposition in the sense of Fish [37] and Fish and Markolefas [38]. Coupling was obtained by linking the FSDT variables, which are present in all the considered models, without using Lagrangian multipliers. The coupling of different kinematic models in the framework of composite beam structure

was presented in [39] by using the extended variational formulation (XVF). In this paper, the sinus model and classical kinematics were coupled into non-overlapping domains.

In Carrera *et al.* [40], a beam model with variable kinematics and global/local features was devised by using the Carrera Unified Formulation (CUF), which was originally developed by Carrera for the analysis multi-layered structures in [41, 42] and allows the automatic implementation of classical to higher-order theories of structures through the use of *fundamental nuclei*. Similarly in the present work, the hierarchical characteristics of CUF are used to develop a new simultaneous multiple-model method for 2D elements with node-dependent kinematics. This node-variable capability given by CUF enables one to vary the kinematic assumptions within the same finite plate element. The expansion order of the plate element is, in fact, a property of the FE node in the present approach. Therefore, between finite elements, the continuity is ensured by adopting the same expansion order in the nodes at the element interface. In this manner, global/local models can be formulated without the use of any mathematical artifice. As a consequence, computational costs can be reduced assuming refined models only in those zones with a quasi-three-dimensional stress field, whereas computationally cheap, low-order kinematic assumptions are used in the remaining parts of the plate structure.

In this paper, the governing equations of the CUF-based variable-kinematics plate element for the linear static analysis of composite structures are derived from the Principle of Virtual Displacement (PVD). Subsequently, FEM is adopted and the Mixed Interpolation of Tensorial Components (MITC) method [43, 44, 45, 46] is used to contrast the shear locking. The developed methodology is, therefore, assessed and used for the analysis of isotropic plates with simply-supported edges and loaded by a uniform pressure, multilayered cantilevered plates with concentrated loads and cross-ply plates with simply-supported edges and subjected to a localized pressure load. The results are compared with various CUF-based theories and, whenever possible, with exact solutions available from the literature.

2 Classical, refined and hierarchical theories for plates

This work proposes a class of new finite elements which allows employing different kinematic assumptions in different subregions of the problem domain. To highlight the capabilities of the novel formulation, a four-node plate elements with node-dependent kinematics is shown in Fig. 1. The element proposed in this example makes use of the Kirchoff's hypothesis at node 1. On the other hand, a second- and a third-order refined theory are employed at node 2 and 3, respectively. Finally, a Reissner-Mindlin plate theory is assumed at node 4. As it will be clear later in this paper, thanks to the hierarchical capabilities of CUF, the choice of the nodal plate theory is arbitrary and variable-kinematics plate elements will be used to implement multi-model methods for global-local analysis.
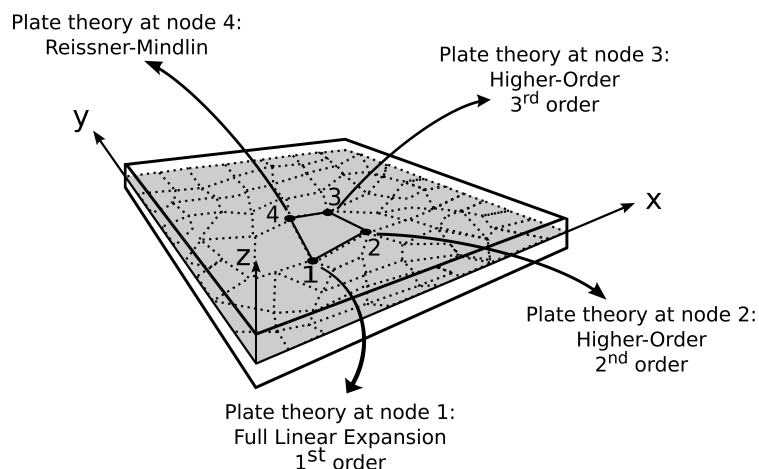

Figure 1: Example of plate element with node-dependent kinematics.

Before discussing the present formulation, a brief overview of classical and higher-order plate theories is given below or the sake of completeness. Plates are bi-dimensional structures in which one dimension (in general the thickness in the z direction) is negligible with respect to the other two dimensions. The geometry and the reference system that is adopted throughout the present work are shown in Fig. 2.
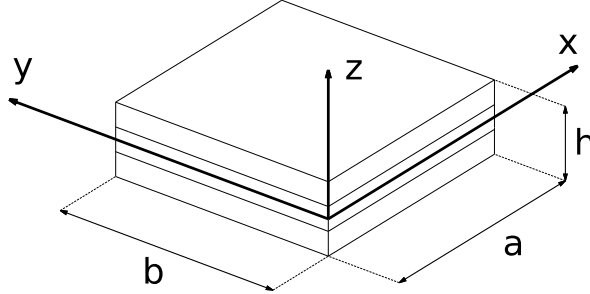
Figure 2: Reference system and geometry of a multilayered plate.

Kirchoff's hypothesis. The simplest plate theory is based on the Kirchoff's hypotheses, and, when applied to composite laminates, it is usually referred to as Classical Lamination Theory (CLT) [1, 2, 3]. In CLT, both transverse shear strains and transverse normal strains are discarded, in usual applications being negligible with respect to the in-plane ones. The displacement field of CLT is represented in Eq. (1) and its geometrical representation is shown in Fig. 3.
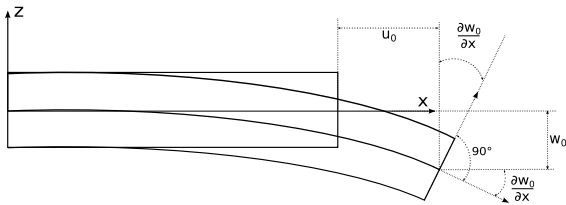
$$
\begin{aligned}
u(x,y,z) &= u_0(x,y) - z\frac{\partial w_0}{\partial x} \\
v(x,y,z) &= v_0(x,y) - z\frac{\partial w_0}{\partial y} \\
w(x,y,z) &= w_0(x,y)
\end{aligned}
\tag{1}
$$

Figure 3: Geometrical representation of the Kirchoff's assumptions.

Reissner-Mindlin theory. Based on the works by Reissner [4] and Mindlin [5], the inclusion of transverse shear strains leads to the plate theory best known as the First-order Shear Deformation Theory (FSDT). The displacement field of the FSDT is represented in Eq. (2) and its geometrical representation is depicted in Fig. 4.
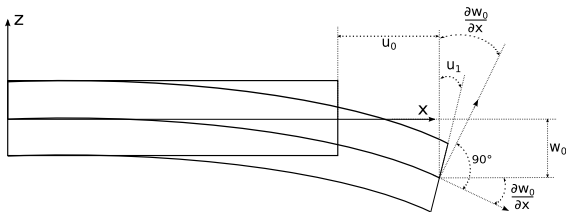
$$
\begin{aligned}
u(x,y,z) &= u_0(x,y) + z\,u_1(x,y) \\
v(x,y,z) &= v_0(x,y) + z\,v_1(x,y) \\
w(x,y,z) &= w_0(x,y)
\end{aligned}
\tag{2}
$$

Figure 4: Geometrical rapresentation of the Reissner-Mindlin theory.

Due to the inconsistency demanded by discarding the transverse normal stress in the material constitutive equations, both CLT and FSDT are no reliable when 3D local effects play a fundamental role, and the correct analysis of the stress field within the structure is needed. To completely remove the inconsistencies of classical plate theories, higher-order expansions of the unknowns with respect to the

z coordinate can be employed.

Higher Order Theories. Classical plate models grant good results when small thickness, homogeneous structures are considered. On the other hand, the analysis of thick plates and multilayered structures may require more sophisticated theories to achieve sufficiently accurate results. As a general guideline, it is clear that the richer the kinematics of the theory, the more accurate the 2D model becomes. In order to overcome the limitations of classical theories, a large variety of plate higher-order theories (HOT) have been proposed in the past and recent literature. Eventually, higher-order theories can be expressed by making use of Taylor-like expansions of the generalized unknowns along the thickness. In the case of generic expansions of N terms, HOT displacement field can be expressed as in Eq. (3). Figure 5 pictorially shows the capabilities of HOT models, which can address complex kinematics in the thickness direction.

$$
\begin{aligned}
u(x,y,z) &= u_0(x,y) + z\,u_1(x,y) + ... + z^N\,u_N(x,y) \\
v(x,y,z) &= v_0(x,y) + z\,v_1(x,y) + ... + z^N\,v_N(x,y) \\
w(x,y,z) &= w_0(x,y) + z\,w_1(x,y) + ... + z^N\,w_N(x,y)
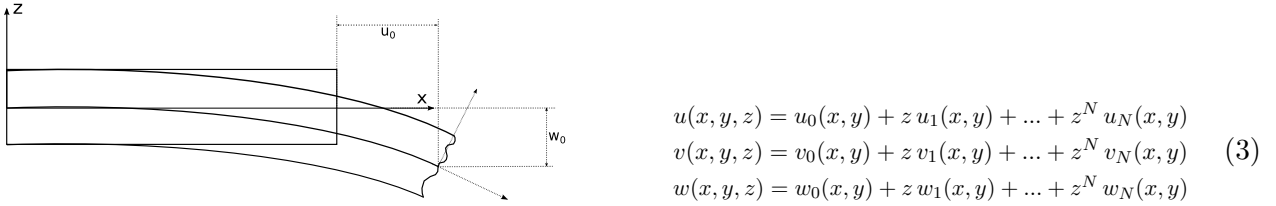\end{aligned}
\quad (3)
$$

Figure 5: Geometrical representation of the Higher Order Theories.

The classical models comprising CLT and FSDT kinematics are particular cases of the full linear expansion, which can be obtained from Eq. (3) by imposing $N = 1$. Nevertheless, the formulation and implementation of classical plate theories as well as their derivation from the full linear model are out of the scope of the present work. Interested readers can find more details on the argument in [47]. However, for the sake of consistency, it should be clarified that the full linear model ($N = 1$ in Eq. (3)) as well as classical theories are affected by the well-known Poisson locking phenomenon. To remedy Poisson locking one may either adopt refined kinematics or use reduced material coefficients in the constitutive relations, by imposing the out-of-plane normal stress to be null. Nevertheless, for the sake of clarity and simplicity of the methodology introduced in this paper, the full linear expansion kinematics ($N = 1$) is not corrected.

Higher Order Theories written in Unified Formulation framework. According to Carrera Unified Formulation (CUF) [47, 42, 48, 49], refined models can be formulated in a straightforward manner by assuming an expansion of each of the primary variables by arbitrary functions in the thickness direction. Thus, each variable can be treated independently from the others, according to the required accuracy. This procedure becomes extremely useful when multifield problems are investigated such as thermoelastic and piezoelectric applications [50, 51, 52, 53]. In a displacement-based formulation, CUF states, in fact, that the three-dimensional displacement field is the combination of through-the-thickness functions weighted by the generalized unknown variables:

$$
\begin{aligned}
u(x,y,z) &= F_0(z)\,u_0(x,y) + F_1(z)\,u_1(x,y) + ... + F_N(z)\,u_N(x,y) \\
v(x,y,z) &= F_0(z)\,v_0(x,y) + F_1(z)\,v_1(x,y) + ... + F_N(z)\,v_N(x,y) \\
w(x,y,z) &= F_0(z)\,w_0(x,y) + F_1(z)\,w_1(x,y) + ... + F_N(z)\,w_N(x,y)
\end{aligned}
\quad (4)
$$

Similarly, in a compact form one has:

$$
\boldsymbol{u}(x,y,z) \; = F_s(z)\boldsymbol{u}_s(x,y) \qquad s = 0, 1, ..., N
\quad (5)
$$

6

where $\boldsymbol{u}(x, y, z)$ is the three-dimensional displacement vector; F_s are the thickness functions depending only on z; $\boldsymbol{u}_s$ is the generalized displacement vector of the variables; s is A sum index; and N is the number of terms of the theory expansion. Depending on the choice of the thickness functions, F_s, and the number of terms in the plate kinematics, N, various theories can be implemented.

Other theories. In this paper, Taylor-like thickness functions are used in the domain of CUF to formulate Equivalent Single Layer (ESL) models as in Eq. (3). ESL models, however, may not be sufficiently accurate to describe adequately the multilayered structures in which, due to their intrinsic anisotropy, the first derivative of the displacement variables in the z-direction is discontinuous. Nevertheless, it is possible to reproduce the zig-zag effects in the CUF-based ESL models by modifying opportunely the F_s functions, for example by adding the Murakami functions [54, 55]. On the other hand, plate models with Layer-Wise (LW) capabilities can be implemented in the framework of CUF by describing the displacement components at the layer level, possibly by using a combination of Lagrange and Legendre-like polynomial as F_s thickness functions [56, 57]. It is important to clarify that the investigation of the effectiveness of the various refined theories for the analysis of composite structures is out of the scope of the present work and more details can be found in [58]. CUF is mainly used here to formulate refined models with node-dependent kinematics to be used for efficient global/local analysis.

3 Finite elements with node-dependent kinematics

Thanks to CUF, FEM arrays of classical to higher-order plate theories can be formulated in a straightforward and unified manner by employing a recursive index notation. By utilizing an FEM approximation, the generalized displacements of Eq. (5) can be expressed as a linear combination of the shape functions to have

$$\boldsymbol{u}_s(x, y) = N_j(x, y)\boldsymbol{u}_{s_j} \qquad j = 1, ..., (\text{nodes per element}) \tag{6}$$

where $\boldsymbol{u}_{s_j}$ is the vector of the generalized nodal unknowns and N_j can be the usual Lagrange shape functions. j denotes a summation on the element nodes. Since the principle of virtual displacements in used in this paper to obtain the elemental FE matrices, it is useful to introduce the finite element approximation of the virtual variation of the generalized displacement vector $\delta\boldsymbol{u}_\tau$,

$$\delta\boldsymbol{u}_\tau(x, y) = N_i(x, y)\delta\boldsymbol{u}_{\tau_i} \qquad i = 1, ..., (\text{nodes per element}) \tag{7}$$

In Eq. (7), δ denotes the virtual variation, whereas indexes τ and i are used instead of s and j, respectively, for the sake of convenience.

In this work, and according to Eqs. (5), (6) and (7), the thickness functions F_s and F_τ, which determine the plate theory order, are independent variables and may change for each node within the plate element. Namely, the three-dimensional displacement field and the related virtual variation can be expressed to address FE node-dependent plate kinematics as follows:

$$\begin{aligned}
\boldsymbol{u}(x, y, z) &= F_s^j(z)N_j(x, y)\boldsymbol{u}_{s_j} & s = 0, 1, ..., N^j & \quad j = 1, ..., (\text{nodes per element}) \\
\delta\boldsymbol{u}(x, y, z) &= F_\tau^i(z)N_i(x, y)\delta\boldsymbol{u}_{\tau_i} & \tau = 0, 1, ..., N^i & \quad i = 1, ..., (\text{nodes per element})
\end{aligned} \tag{8}$$

where the subscripts τ, s, i, and j denote summation. Superscripts i and j denote node dependency, such that for example F_τ^i is the thickness expanding function and N^i is the number of expansion terms at node i, respectively.

For the sake of clarity, the displacement field of the variable kinematic plate element as discussed in Fig. 1 is described in detail hereafter. The same plate element is represented in Fig. 6, which also shows the though-the-thickness kinematics at the nodal level. The global displacement field of the element is approximated as follows:

- Node 1   Plate Theory = HOT with $N^1 = 1$ Eq. (3)

- Node 2   Plate Theory = HOT with $N^2 = 2$ Eq. (3)

- Node 3   Plate Theory = HOT with $N^3 = 3$ Eq. (3)

- Node 4   Plate Theory = FSDT   Eq. (2)

In a CUF-based FE framework and according to Eq. (8), it is easy to verify that the displacements at a generic point belonging to the plate element can be expressed as given in Eq. (9). In this equation, only the displacement component along x-axis is given for simplicity reasons:

$$
\begin{aligned}
u(x,y,z) = {} & \left(u_{0_1} + z\, u_{1_1}\right) N_1(x,y) + \left(u_{0_2} + z\, u_{1_2} + z^2\, u_{2_2}\right) N_2(x,y) \\
& + \left(u_{0_3} + z\, u_{1_3} + z^2\, u_{2_3} + z^3\, u_{3_3}\right) N_3(x,y) + \left(u_{0_4} + z\, u_{1_4}\right) N_4(x,y)
\end{aligned}
\tag{9}
$$

It is intended that, due to node-variable expansion theory order, the assembling procedure of each finite element increases in complexity with respect to classical mono-theory finite elements. In the present FE approach, in fact, it is clear that both rectangular and square arrays are handled and opportunely assembled for obtaining the final elemental matrices.
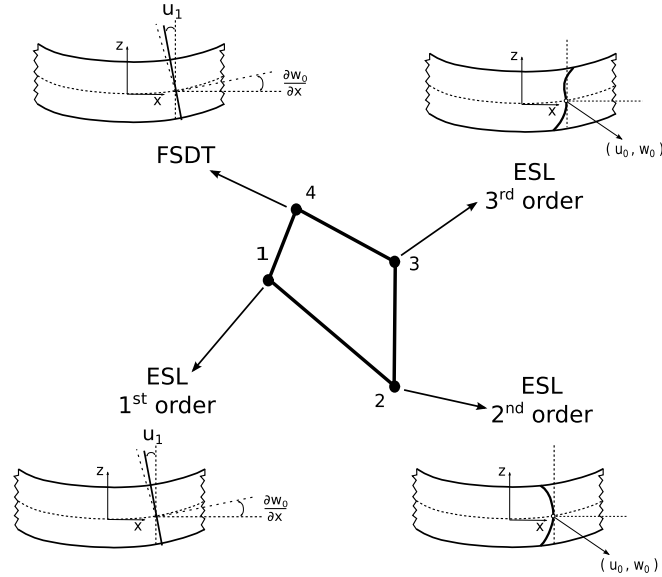

Figure 6: Displacement field at the nodal level. Plate element with node-dependent kinematics.

3.1   Fundamental nucleus of the stiffness matrix

Given CUF and FE approximation, the governing equations for the static response analysis of the multi-layer plate structure can be obtained by using the principle of virtual displacements, which states:

$$
\int_{\Omega} \int_{A} \delta \boldsymbol{\epsilon}^T \boldsymbol{\sigma} \, d\Omega \, dz = \delta L_e
\tag{10}
$$

where the term on the left-hand side represents the virtual variation of the strain energy; Ω and A are the integration domains in the plane and the thickness direction, respectively; $\boldsymbol{\epsilon}$ and $\boldsymbol{\sigma}$ are the vector of the strain and stress components; and δL_e is the virtual variation of the external loadings. By substituting the constitutive equations for composite elastic materials, the linear geometrical relations

as well as Eq. (8) into Eq. (10), the linear algebraic system in the form of governing equations is obtained in the following matrix expression:

$$\delta \boldsymbol{u}_{\tau_i}: \quad \boldsymbol{K}^{\tau s i j} \boldsymbol{u}_{s_j} = \quad \boldsymbol{P}^{s j} \tag{11}$$

where $\boldsymbol{K}^{\tau s i j}$ and $\boldsymbol{P}^{s j}$ are the element stiffness and load FE arrays written in the form of *fundamental nuclei*. In particular, $\boldsymbol{K}^{\tau s i j}$ is a 3×3 matrix whose components are given in the following:

$$K_{xx}^{\tau i s j} = \int_{\Omega} N_i N_j \, d\Omega \int_A C_{55} \, F_{\tau,z}^i F_{s,z}^j \, dz + \int_{\Omega} N_{i,y} N_{j,y} \, d\Omega \int_A C_{66} \, F_\tau^i F_s^j \, dz + \int_{\Omega} N_{i,x} N_{j,y} \, d\Omega \int_A C_{16} \, F_\tau^i F_s^j \, dz + $$
$$+ \int_{\Omega} N_{i,y} N_{j,x} \, d\Omega \int_A C_{16} \, F_\tau^i F_s^j \, dz + \int_{\Omega} N_{i,x} N_{j,x} \, d\Omega \int_A C_{11} \, F_\tau^i F_s^j \, dz$$

$$K_{xy}^{\tau i s j} = \int_{\Omega} N_i N_j \, d\Omega \int_A C_{45} \, F_{\tau,z}^i F_{s,z}^j \, dz + \int_{\Omega} N_{i,y} N_{j,y} \, d\Omega \int_A C_{26} \, F_\tau^i F_s^j \, dz + \int_{\Omega} N_{i,x} N_{j,y} \, d\Omega \int_A C_{12} \, F_\tau^i F_s^j \, dz + $$
$$+ \int_{\Omega} N_{i,y} N_{j,x} \, d\Omega \int_A C_{66} \, F_\tau^i F_s^j \, dz + \int_{\Omega} N_{i,x} N_{j,x} \, d\Omega \int_A C_{16} \, F_\tau^i F_s^j \, dz$$

$$K_{xz}^{\tau i s j} = \int_{\Omega} N_i N_{j,y} \, d\Omega \int_A C_{45} \, F_{\tau,z}^i F_s^j \, dz + \int_{\Omega} N_i N_{j,x} \, d\Omega \int_A C_{55} \, F_{\tau,z}^i F_s^j \, dz + \int_{\Omega} N_{i,y} N_j \, d\Omega \int_A C_{36} \, F_\tau^i F_{s,z}^j \, dz + $$
$$+ \int_{\Omega} N_{i,x} N_j \, d\Omega \int_A C_{13} \, F_\tau^i F_{s,z}^j \, dz$$

$$K_{yx}^{\tau i s j} = \int_{\Omega} N_i N_j \, d\Omega \int_A C_{45} \, F_{\tau,z}^i F_{s,z}^j \, dz + \int_{\Omega} N_{i,y} N_{j,y} \, d\Omega \int_A C_{26} \, F_\tau^i F_s^j \, dz + \int_{\Omega} N_{i,x} N_{j,y} \, d\Omega \int_A C_{66} \, F_\tau^i F_s^j \, dz + $$
$$+ \int_{\Omega} N_{i,y} N_{j,x} \, d\Omega \int_A C_{12} \, F_\tau^i F_s^j \, dz + \int_{\Omega} N_{i,x} N_{j,x} \, d\Omega \int_A C_{16} \, F_\tau^i F_s^j \, dz$$

$$K_{yy}^{\tau i s j} = \int_{\Omega} N_i N_j \, d\Omega \int_A C_{44} \, F_{\tau,z}^i F_{s,z}^j \, dz + \int_{\Omega} N_{i,y} N_{j,y} \, d\Omega \int_A C_{22} \, F_\tau^i F_s^j \, dz + \int_{\Omega} N_{i,x} N_{j,y} \, d\Omega \int_A C_{26} \, F_\tau^i F_s^j \, dz + $$
$$+ \int_{\Omega} N_{i,y} N_{j,x} \, d\Omega \int_A C_{26} \, F_\tau^i F_s^j \, dz + \int_{\Omega} N_{i,x} N_{j,x} \, d\Omega \int_A C_{66} \, F_\tau^i F_s^j \, dz$$

$$K_{yz}^{\tau i s j} = \int_{\Omega} N_i N_{j,y} \, d\Omega \int_A C_{44} \, F_{\tau,z}^i F_s^j \, dz + \int_{\Omega} N_i N_{j,x} \, d\Omega \int_A C_{45} \, F_{\tau,z}^i F_s^j \, dz + \int_{\Omega} N_{i,y} N_j \, d\Omega \int_A C_{23} \, F_\tau^i F_{s,z}^j \, dz + $$
$$+ \int_{\Omega} N_{i,x} N_j \, d\Omega \int_A C_{36} \, F_\tau^i F_{s,z}^j \, dz$$

$$K_{zx}^{\tau i s j} = \int_{\Omega} N_i N_{j,y} \, d\Omega \int_A C_{36} \, F_{\tau,z}^i F_s^j \, dz + \int_{\Omega} N_i N_{j,x} \, d\Omega \int_A C_{13} \, F_{\tau,z}^i F_s^j \, dz + \int_{\Omega} N_{i,y} N_j \, d\Omega \int_A C_{45} \, F_\tau^i F_{s,z}^j \, dz + $$
$$+ \int_{\Omega} N_{i,x} N_j \, d\Omega \int_A C_{55} \, F_\tau^i F_{s,z}^j \, dz$$

$$K_{zy}^{\tau i s j} = \int_{\Omega} N_i N_{j,y} \, d\Omega \int_A C_{23} \, F_{\tau,z}^i F_s^j \, dz + \int_{\Omega} N_i N_{j,x} \, d\Omega \int_A C_{36} \, F_{\tau,z}^i F_s^j \, dz + \int_{\Omega} N_{i,y} N_j \, d\Omega \int_A C_{44} \, F_\tau^i F_{s,z}^j \, dz + $$
$$+ \int_{\Omega} N_{i,x} N_j \, d\Omega \int_A C_{45} \, F_\tau^i F_{s,z}^j \, dz$$

$$K_{zz}^{\tau i s j} = \int_\Omega N_i N_j \, d\Omega \int_A C_{33} F_{\tau,z}^i F_{s,z}^j \, dz + \int_\Omega N_{i,y} N_{j,y} \, d\Omega \int_A C_{44} F_\tau^i F_s^j \, dz + \int_\Omega N_{i,x} N_{j,y} \, d\Omega \int_A C_{45} F_\tau^i F_s^j \, dz +$$

$$+ \int_\Omega N_{i,y} N_{j,x} \, d\Omega \int_A C_{45} F_\tau^i F_s^j \, dz + \int_\Omega N_{i,x} N_{j,x} \, d\Omega \int_A C_{55} F_\tau^i F_s^j \, dz$$

where comma denote partial derivatives and C_{11}, C_{12}, ..., C_{66} are the material coefficients for a monoclinic lamina as defined in [59].

The fundamental nucleus as given above is the basic building block for the construction of the element stiffness matrix of classical, refined and variable-kinematic theories. In fact, given these nine components, element stiffness matrices of arbitrary plate models can be obtained in an automatic manner by expanding the fundamental nucleus versus the indexes τ, s, i, and j. In the development of ESL theories as in the case of this paper, the fundamental nucleus of the stiffness matrix is evaluated at the layer level and then assembled as shown in Fig. 7. This figure, in particular, illustrates the expansion of the fundamental nucleus in the case of a 9-node Lagrange finite element with node-by-node variable kinematics, as in the case of this paper. It must be added that, in this work, an MITC technique is used to overcome the shear locking phenomenon, see [53]. However, for more details about the explicit formulation of the CUF fundamental nuclei, interested readers are referred to the recent book by Carrera *et al.* [47].
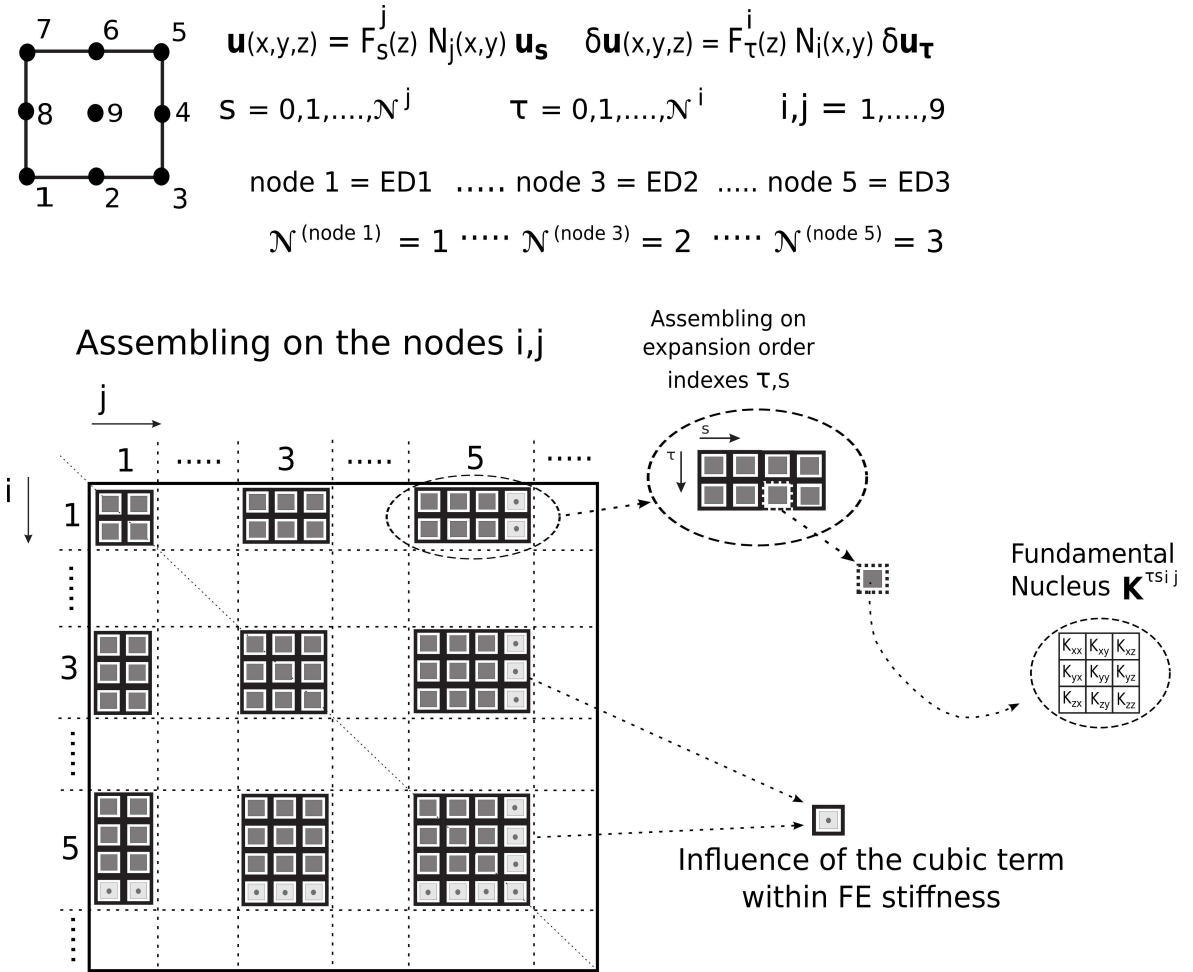

Figure 7: Assembling scheme of a 9-node finite element with node-dependent kinematics. Highlights of the influence of the cubic term of a 3rd order Taylor expansion model in the FE stiffness.

4 Numerical results

Some problems have been considered to assess the capabilities of the proposed variable-kinematics plate elements and related global/local analysis. These analysis cases comprise both metallic and composite laminated plate structures with different boundary conditions and loadings. Whenever possible, the proposed multi-theory models are compared to single-theory refined elements. According to CUF terminology, the latter models are referred to as EDN, where E stands for Equivalent Single Layer (ESL), D denotes the fact that displacement-based principle of virtual work is used for the formulation of the governing equations, and N is the theory approximation order. Eventually, Layer-wise models are used for comparison and, in this case, the letter L is used instead of E in the notation mentioned above. If a Navier-type closed form solution is employed instead of FEM, the subscript (a) is used. On the contrary, for the sake of clarity, multi-model theories are opportunely described for each numerical case considered.

4.1 Simply-supported isotropic plate under localized pressure load

A simply-supported isotropic plate is analysed first. The geometrical dimensions are: $a = 2\,m$, $b = h = 0.2\,m$. The employed material is isotropic with Young modulus equal to $E = 75\,GPa$ and Poisson ratio $\nu = 0.3$. The plate is simply-supported along two opposite sides and free along the remaining two edges. It undergoes a localised uniform pressure, $P = 1\,Pa$, acting on the 10% of the length and centered at the mid-span, see Fig. 8(a). The transverse section of the proposed structure is shown in Fig. 8(b), where the verification points at which displacement and stress components are measured are also depicted. The results of the present methodology, in fact, are compared with some solutions from the literature and with an MSC/NASTRAN solid model made of 8-node CHEXA elements. With reference to Fig. 8(b), the in-plane displacements u and shear stress component σ_{xz} are evaluated at $x = 0$, whereas the other two displacement components v and w and the normal stresses σ_{xx} and σ_{zz} are evaluated at plate mid-span. The results are given in the following non-dimensional form:

$$(\hat{u}, \hat{v}, \hat{w}) = \frac{Eh}{a^2 P}\,(u, v, w) \qquad (\hat{\sigma}_{xx}, \hat{\sigma}_{xz}, \hat{\sigma}_{zz}) = \frac{1}{P}\,(\sigma_{xx}, \sigma_{xz}, \sigma_{zz}) \tag{12}$$
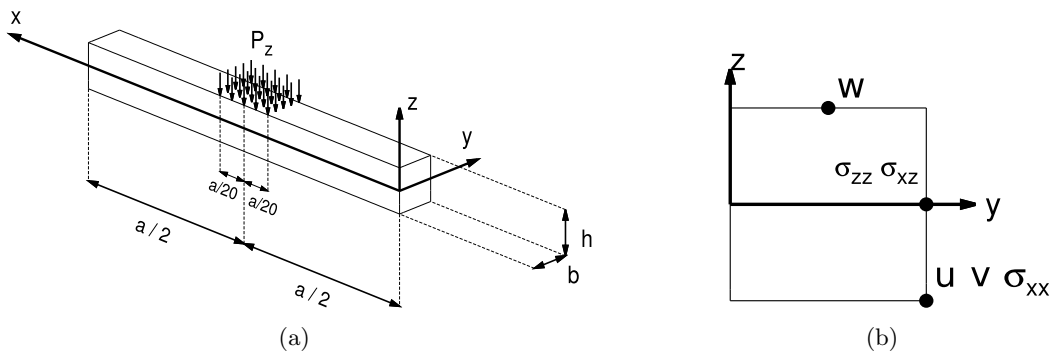

Figure 8: Reference system of the isotropic plate (a), and placement of the evaluation points on the transverse section (b).

First, a convergence study is conducted. To serve this scope and as shown in Fig. 9, the plate structure has been subdivided into 5 zones along the axis x, and they are numbered from 1 to 3 for symmetry reasons. The choice of dividing the structure in this manner was made for allowing fair comparisons with other models from the literature [33, 24]. According to Table 1, which shows the converge study of the single-theory ED4 CUF model for various mesh discretizations and related

comparison with different solid models from MSC/NASTRAN, a non-uniform mesh grid of 20×4 elements is enough for ensuring good results. The same mesh is depicted in Fig. 9 and it is used in the remaining analyses for the definition of the CUF-based single- and multi-theory models.
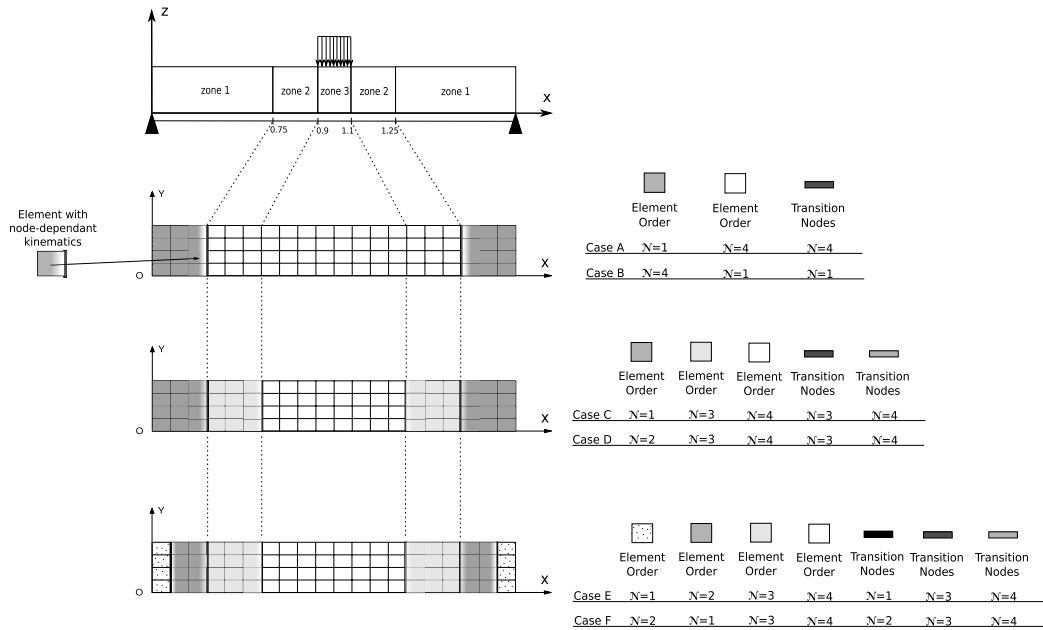

Figure 9: Subdivision zones for the isotropic plate, final mesh grid chosen after convergence study, and graphical description of the multi-theory models.

Table 1: Convergence study according to the $ED4$ model of the isotropic plate structure.

	$(-10)\,\hat{u}$	$(-10^2)\,\hat{v}$	$(-1)\,\hat{w}$	$(10^{-1})\,\hat{\sigma}_{xx}$	$(-10)\,\hat{\sigma}_{xz}$	$(-10)\,\hat{\sigma}_{zz}$	$DOFs^*$
$Mesh\,10\times4$							
$zone1$ $zone2$ $zone3$	3.743	2.129	2.544	1.440	8.640	5.287	2835
2×4 2×4 2×4							
$Mesh\,16\times4$							
$zone1$ $zone2$ $zone3$	3.744	2.126	2.544	1.431	8.641	5.247	4455
3×4 3×4 4×4							
$Mesh\,20\times4$							
$zone1$ $zone2$ $zone3$	3.743	2.126	2.544	1.431	8.641	5.248	5535
4×4 4×4 4×4							
$Mesh\,20\times8$							
$zone1$ $zone2$ $zone3$	3.743	2.126	2.544	1.431	8.637	5.254	10455
4×8 4×8 4×8							
$Mesh\,30\times4$							
$zone1$ $zone2$ $zone3$	3.743	2.125	2.544	1.429	8.641	5.263	8235
6×4 6×4 6×4							
$Mesh\,20\times4$							
$zone1$ $zone2$ $zone3$	3.743	2.125	2.544	1.429	8.641	5.267	5535
3×4 3×4 8×4							
$8node\,SOLID$ $Mesh\,100\times20\times20$	3.788	2.124	2.544	1.352	8.402	5.202	131859
$8node\,SOLID$ $Mesh\,100\times40\times40$	3.667	2.124	2.544	1.389	8.502	5.216	502619
$8node\,SOLID$ $Mesh\,80\times40\times40$	3.440	2.124	2.544	1.388	8.502	5.197	401759
$8node\,SOLID$ $Mesh\,100\times60\times60$	3.776	2.124	2.544	1.402	8.533	5.221	1112579

*: Degrees of freedom of the whole plate structure

Table 2 shows the results for the present metallic plate from various single- and multi-theory CUF models. Solutions from the literature [33, 24] are also given for comparison. Multi-theory models are referred to as $Case\,A$ to $Case\,F$, and they are defined according to Fig. 9. In particular, in $Case\,A$, lower-order kinematics is employed at the plate boundaries, whereas 4-th order plate theory is used close to the loading. Vice-versa, in $Case\,B$, refined approximation orders are utilized close to the boundary. The present $Case\,A$ and $Case\,B$ multi-theory models are analogous to models $Arlequin^A$ and $Arlequin^B$ from [33], where the Arlequin method was used to mix finite beam elements with different kinematics at the interface, and LM^A and LM^B from [24], where Lagrange multipliers were used along with 1D CUF to implement variable kinematic beam theories. Results from other original global/local plate models referred to as $Case\,C$ to $Case\,F$ are also given in Table 2 and they are graphically explained in Fig. 9. In this table, the present results are also compared to a 3D solid solution and 1D mono-models, which are referred to as $TE1$ - $TE4$ and are CUF beam models based on N-order Taylor expansions of the displacement field over the beam cross-section (see [24]). All the multi-theory models in this paper have been implemented by making use of the node-by-node variable kinematic formulation encompassed in the domain of CUF. In this methodology, structural domains with lower- and higher-order theories are coupled by enforcing the same kinematics at the interface nodes. In this manner, there is no information loss and no need to adopt any mathematical artifice, such as Lagrange multipliers or *overlapping regions*.

Table 2: Simply-supported metallic plate. Displacement and stress components from single-theory, multi-theory and reference models.

	$(-10)\,\hat{u}$	$(-10^2)\,\hat{v}$	$(-1)\,\hat{w}$	$(10^{-1})\,\hat{\sigma}_{xx}$	$(-10)\,\hat{\sigma}_{xz}$	$(-10)\,\hat{\sigma}_{zz}$	$DOFs^*$
			Reference solutions [33]				
$SOLID$	3.776	2.124	2.544	1.402	8.533	5.221	558150
$Arlequin^A$	3.729	2.116	2.537	1.424	5.000	5.217	1197
$Arlequin^B$	3.716	-0.056	2.547	1.444	8.352	4.807	1197
LM^A	3.699	2.116	2.524	1.420	5.000	6.001	1134
LM^B	3.732	-0.080	2.550	1.419	8.429	4.395	1134
$TE4$	3.735	2.116	2.542	1.423	8.511	6.003	2745
$TE3$	3.735	2.092	2.542	1.425	8.462	6.063	1830
$TE2$	3.729	2.108	2.532	1.409	5.865	4.265	1098
$TE1$	3.736	-0.080	2.548	1.419	5.000	4.395	549
			Present single- and multi-theory models				
$ED4$	3.743	2.125	2.544	1.429	8.641	5.267	2835
$ED3$	3.742	2.139	2.544	1.434	8.641	5.286	2268
$ED2$	3.731	2.097	2.534	1.402	6.262	5.087	1701
$ED1$	3.402	2.688	2.323	1.414	6.265	4.594	1134
$Case\,A$	3.562	2.125	2.460	1.429	6.265	5.267	2349
$Case\,B$	3.587	2.688	2.413	1.414	8.708	4.594	1620
$Case\,C$	3.561	2.125	2.460	1.429	6.256	5.275	2187
$Case\,D$	3.731	2.125	2.537	1.429	6.263	5.276	2349
$Case\,E$	3.704	2.125	2.532	1.429	6.358	5.276	2133
$Case\,F$	3.591	2.125	2.465	1.429	6.154	5.275	2133

$*$: for a fair comparison with reference solutions, DOFs are given for half plate structure

Additional results in terms of transverse displacement w, in-plane stress σ_{xx}, transverse shear stress σ_{xz} and transverse normal stress σ_{zz} along the thickness are represented in Fig. 10, 11, 12, and 13, respectively. The following comments can be drawn from the analysis:

- Single-theory models with lower expansion order, i.e. $ED1$ and $ED2$, yield good results in terms of displacements and in-plane stress, σ_{xx}. However, in order to accurately describe the shear and normal transverse stresses σ_{xz} and σ_{zz}, higher-order theories, such as $ED3$ and $ED4$, are required.

- Depending on the structural domain of interest, multi-theory models allow us to enrich the solution in a smart and efficient manner. Nevertheless, accurate analysis may require attentive distribution of the kinematics approximation through the problem domain. For example, although $Case\,E$ and $Case\,F$ models have the same number of DOFs and according to Fig. 10, the distribution of the transverse displacement w through the thickness can vary significantly. Contrarily, the in-plane stress σ_{xx} is not sensitive to variable-kinematic modeling, see Fig. 11.

- As further guidelines, it is clear from Fig. 12 that, as far as the accuracy on the transverse shear stress σ_{xz} is concerned, higher-order approximation theories must be placed close to the boundaries. This is the case of the $Case\,B$ model and mono-theory models $ED3$ and $ED4$. Contrarily, if good approximation of the transverse normal stress σ_{zz} is needed, the model kinematic order must be enriched in the loading zone. Except for $Case\,B$ configuration and mono-model $ED1$,

14

all the other cases have a good behaviour in terms of σ_{zz}, see Fig. 13. It has to be noticed that $Case\,A$ and $Case\,C$ to $Case\,F$, have the same accuracy as the reference mono-theory model $ED4$.
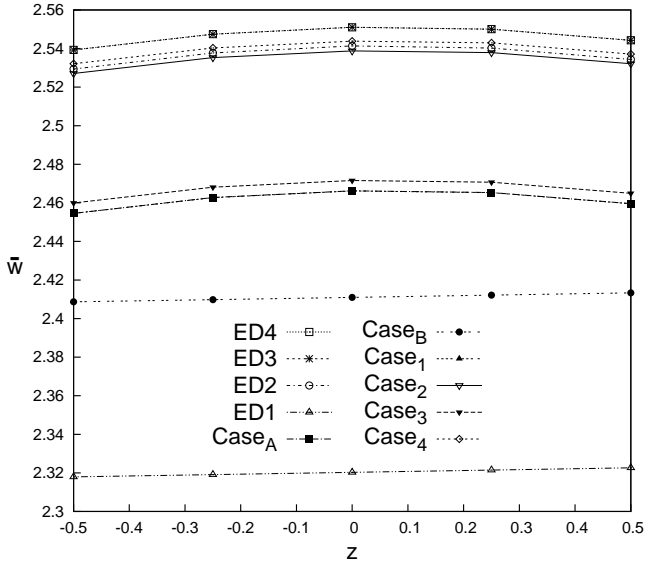

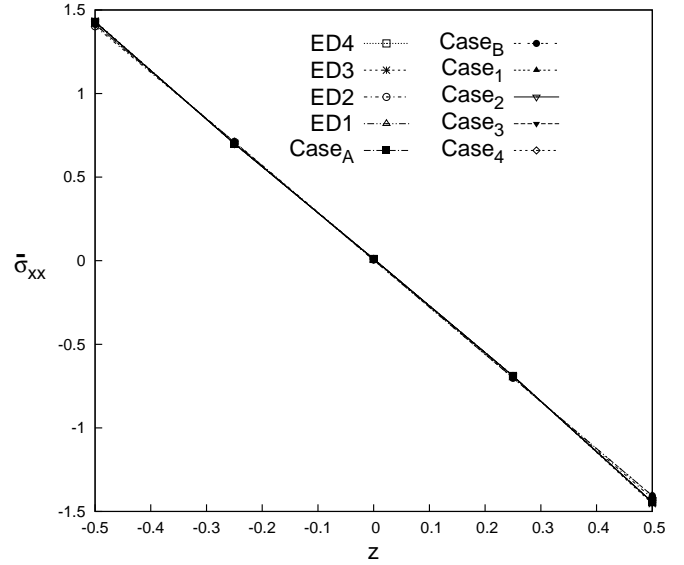Figure 10: Transverse displacement $w(x;y) = w(a/2;b/2)$. Isotropic plate.

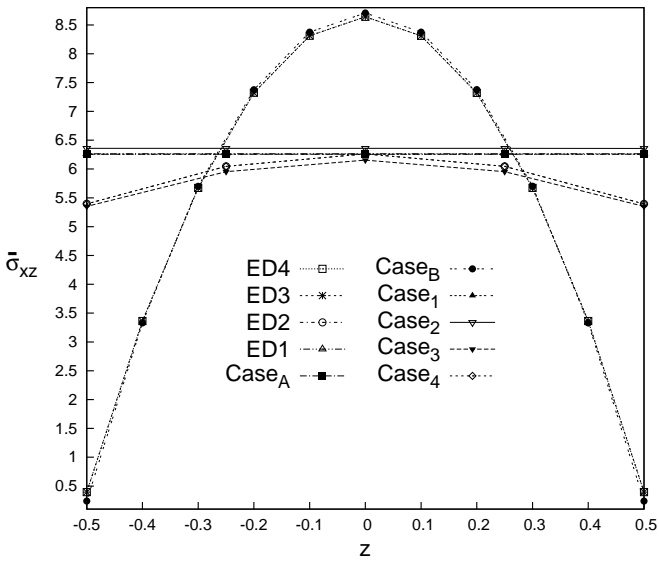Figure 11: In-plane stress $\sigma_{xx}(x;y) = \sigma_{xx}(a/2;b)$. Isotropic plate.

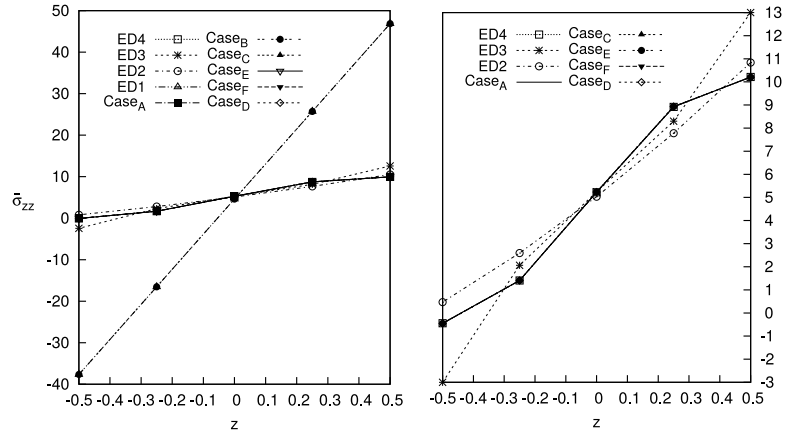Figure 12: Transverse shear stress $\sigma_{xz}(x;y) = \sigma_{xz}(0;b)$. Isotropic plate.

Figure 13: Transverse normal stress $\sigma_{zz}(x;y) = \sigma_{zz}(a/2;b)$. Isotropic plate.

For the sake of completeness, the distribution of transverse shear stress σ_{xz}, see Fig. 14, and transverse normal stress σ_{zz}, see Fig. 15, along the in-plane x axis are given. The results demonstrate that the $Case\,A$ model can represent the transverse shear stress σ_{xz} accurately only in the loading zone. On the other hand, the same model gives an error of approximately 28% in the remaining part of the domain with respect to $Case\,B$ and $ED4$ models. Regarding the transverse normal stress σ_{zz} distribution along x, it is evident that higher-order models are required to describe the solution

15

correctly. Even in this case, *Case A* model can represent a correct behaviour in the loading zone only. For consistency reasons, a convergence analysis with respect to the size of the transition elements is made for the analysis cases discussed in Figs. 14 and 15. The convergence analysis is performed keeping the same mesh of the original cases, but reducing the size of the transition elements in the x direction. The original size of the transition zone is $El_x = 0,25$ m, whereas in the convergence analysis proposed in Fig. 16 transition zones as long as 0.03 m and 0.15 m are chosen. From the convergence analysis, it is clear that, in the case of σ_{xz} stress component, increasing oscillations of the solution appear as the size of the transition zone is reduced. On the contrary, the solution in terms of transverse normal stress σ_{zz} is much smooth if short transition zones are employed. Nevertheless, it must be underlined that the stress field within the inner local region of the analysis domain is not influenced by the choice of the length of the transition zone.
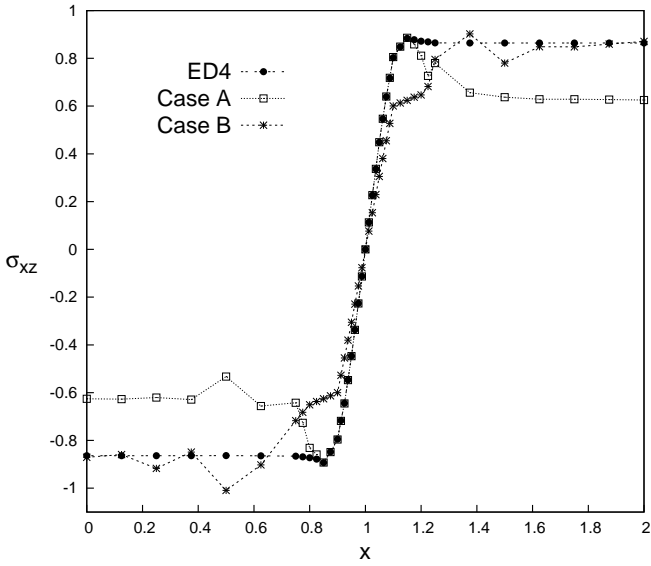

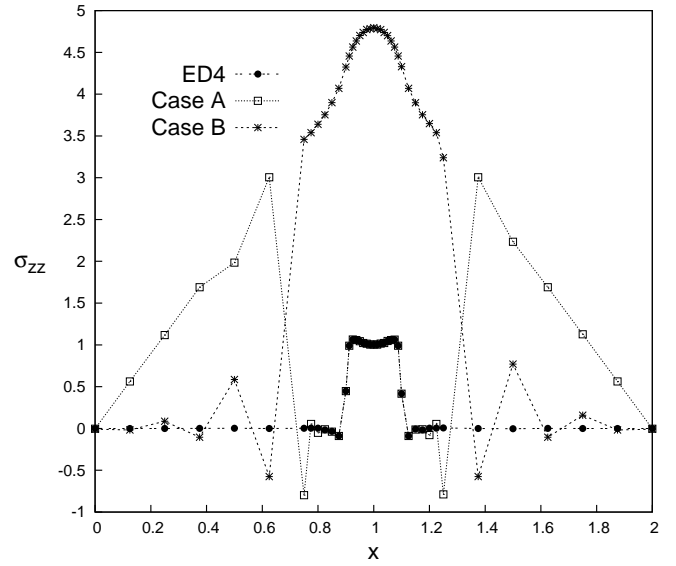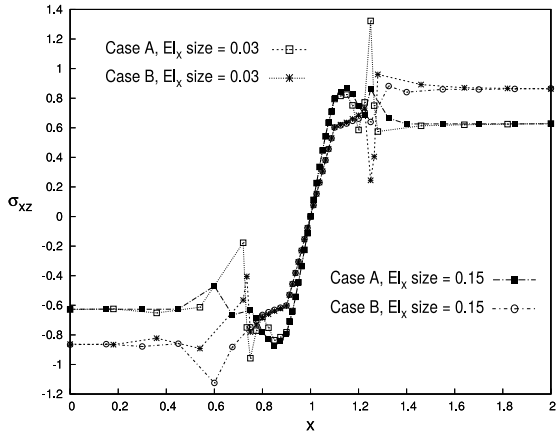Figure 14: Transverse shear stress $\sigma_{xz}(y;z) = \sigma_{xz}(b;0)$ along the beam axis. Isotropic plate.
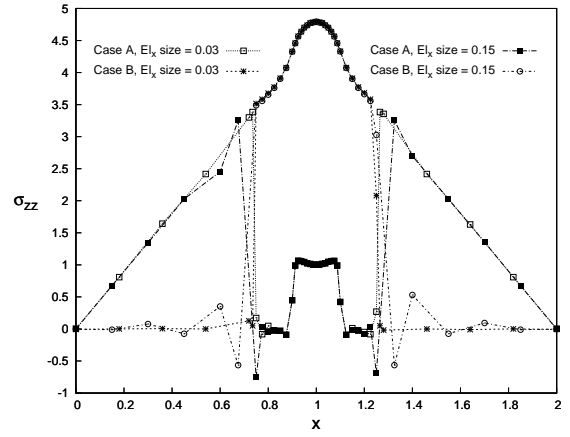

Figure 15: Transverse normal stress $\sigma_{zz}(y;z) = \sigma_{zz}(b/2;h/2)$ along the beam axis. Isotropic plate.

16

(a) Transverse shear stress $\sigma_{xz}(y;z) = \sigma_{xz}(b;0)$ along the beam axis.

(b) Transverse normal stress $\sigma_{zz}(y;z) = \sigma_{zz}(b/2;h/2)$ along the beam axis.

Figure 16: Convergence analysis of the transition elements for the transverse shear and normal stresses along the beam axis.

Finally, in order to show the 3D capabilities of the proposed methodology, the three-dimensional distribution of the shear stress σ_{xz} and the normal stress σ_{zz} are shown in Figs. 17 and 18, respectively, where the results from a solid model by MSC/NASTRAN are compared with $ED4$ single-theory plate model and $Case\,A$ and $Case\,B$ multi-theory models. From a comparison of the proposed variable-kinematic models with respect to the $ED4$ plate model and the solid solution, it is possible to observe a possible reduction of DOFs equal to 18% and 99%, respectively. Moreover, if accurate solutions are needed only in localized zones of the structure, even more efficient models can be implemented with the present approach.
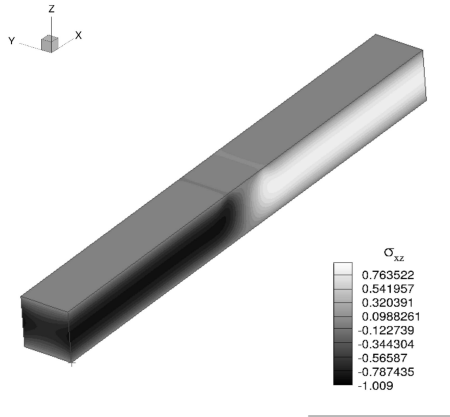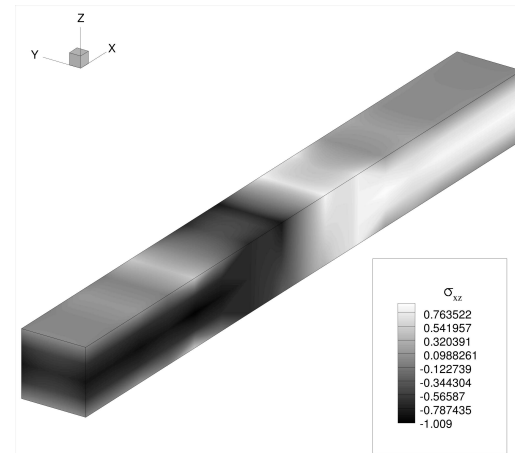
(a) MSC/NASTRAN 3D SOLID model
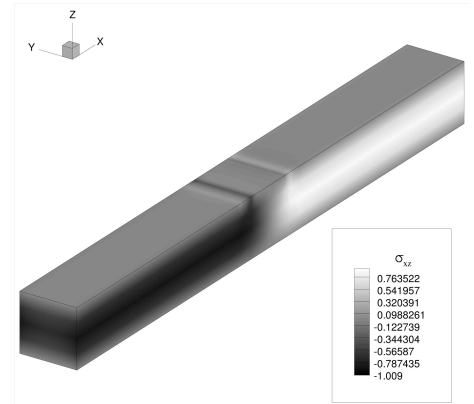
(b) *ED4*
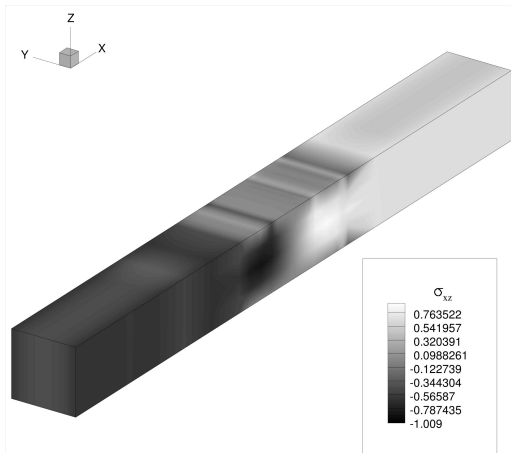
(c) *Case A* multi-theory model

(d) *Case B* multi-theory model

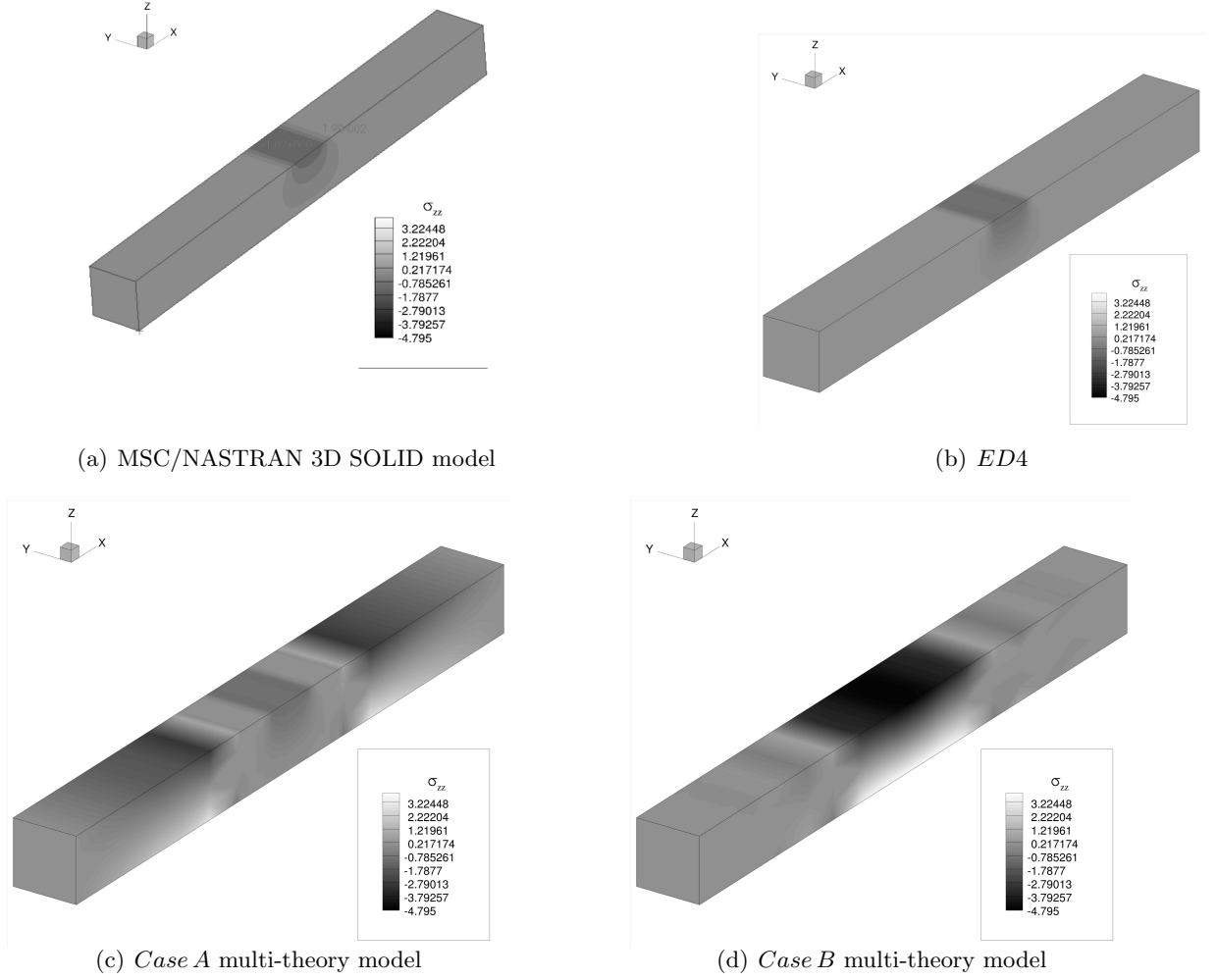Figure 17: Three-dimensional representation of the transverse shear stress $\boldsymbol{\sigma}_{xz}$. Isotropic plate.

(a) MSC/NASTRAN 3D SOLID model

(b) $ED4$

(c) $Case\,A$ multi-theory model

(d) $Case\,B$ multi-theory model

Figure 18: Three-dimensional representation of the transverse normal stress $\boldsymbol{\sigma}_{zz}$. Isotropic plate.

4.2 Eight-layer cantilever plate

A cantilever eight-layer plate is analysed as the second example and it is shown in Fig. 19. The structure is loaded at the free end with a concentrated load equal to $P_z = -0.2\,N$. The geometrical dimensions are: $a = 90\,mm$, $b = 1\,mm$, $h = 10\,mm$. The mechanical properties of the material labeled with the number 1 are: $E_L = 30\,GPa$, $E_T = 1\,GPa$, $G_{LT} = G_{TT} = 0.5\,GPa$, $\nu_{LT} = \nu_{TT} = 0.25$. On the other hand, the mechanical properties of the material labeled with the number 2 are: $E_L = 5\,GPa$, $E_T = 1\,GPa$, $G_{LT} = G_{TT} = 0.5\,GPa$, $\nu_{LT} = \nu_{TT} = 0.25$. As clear from Fig. 19, the material stacking sequence is $[1/2/1/2]_s$.

First, a convergence study on a single-theory plate model was performed. As far as an $ED4$ model is concerned and as shown in Table 3, a mesh grid of 12×2 elements is enough to ensure convergent results. Various node-variable kinematic CUF models have been used to perform the global/local analysis of the proposed plate structure, and they are depicted in Fig. 20. These models are compared in Table 4 with lower- to higher-order single-theory models as well as with various solutions from the literature, including an analytical solution based on the 2D elasticity as presented in Lekhnitskii [60]. It can be observed that mono-theory models with lower expansion order, $ED1$ and $ED2$, yield

good results for the transverse displacements w and the in-plane stress σ_{xx}. However, in order to accurately describe the shear transverse stresses σ_{xz}, higher-order mono-model theories, $ED3$ and $ED4$, are required. Nevertheless, accurate solutions in localized regions/points can be obtained by using variable kinematics, see $Case\,A$ to $Case\,C$.
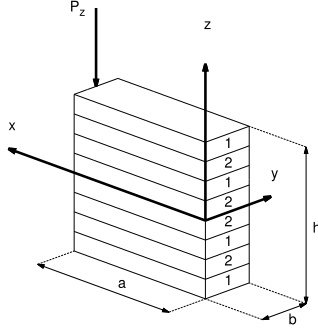

Figure 19: Reference system of the eight-layer plate with concentrated loading. The material lamination scheme is indicated with label 1 and label 2.
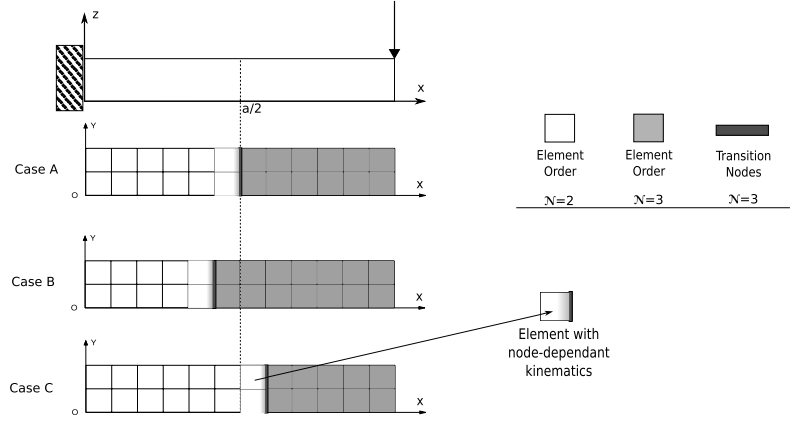

Figure 20: Multi-theory models of the eight-layer plate by finite plate elements with node-dependent kinematics.

Table 3: Convergence study versus the number of elements of the $ED4$ single-theory model of the eight-layer cantilever plate. Transverse displacement $w = -10^2 \times w(a, b/2, 0)$, in-plane principal stress $\sigma_{xx} = 10^3 \times \sigma_{xx}(a/2, b/2, +h/2)$, transverse shear stress $\sigma_{xz} = 10^2 \times \sigma_{xz}(a/2, b/2, 0)$.

	Mesh	2×2	4×2	6×2	8×2	10×2	12×2
	w	3.029	3.029	3.029	3.028	3.028	3.028
$ED4$	σ_{xx}	684	723	729	730	731	731
	σ_{xz}	3.054	2.829	2.820	2.821	2.822	2.822

20

Table 4: Eight-layer cantilever plate. Transverse displacement $w = w(a, b/2, 0)$, in-plane normal stress $\sigma_{xx} = \sigma_{xx}(a/2, b/2, +h/2)$, transverse shear stress $\sigma_{xz} = \sigma_{xz}(a/2, b/2, 0)$ by various single- and multi-theory models.

	$(-10^2)\, w$	$(10^3)\, \sigma_{xx}$	$(10^2)\, \sigma_{xz}$	$DOFs$
Reference solutions				
Nguyen and Surana [61]	3.031	720		
Davalos *et al.* [62]	3.029	700		
Xiaoshan [63]	3.060	750		
Vo and Thai [64]	3.024			
Lekhnitskii [60]		730	2.789	
Present single- and multi-theory models				
$LD4$	3.030	730	2.789	12375
$ED4$	3.028	731	2.822	1875
$ED3$	3.027	731	2.822	1500
$ED2$	2.980	731	2.005	1125
$ED1$	2.981	729	2.000	750
$Case\,A$	3.004	867	2.248	1320
$Case\,B$	3.010	737	2.781	1365
$Case\,C$	3.002	731	2.030	1305

Some results in terms of transverse displacement w, transverse shear stress σ_{xz} and in-plane stress σ_{xx} along the thickness are represented in Figs. 21, 22 and 23, respectively. Some more comments can be made:

- As shown in Fig. 21, the through-the-thickness distribution of the transverse displacement w, evaluated at the free tip of the plate, is correctly predicted by a third-order model. The same accuracy cannot be reached by the proposed models with node-variable kinematics.

- Figure 22 shows that the transverse shear stress σ_{xz}, evaluated at the mid-span of the plate, is very sensitive to the position of the transition variable-kinematic elements. $Case\,B$ model has the same accuracy as mono-model $ED3$ and $ED4$. On the contrary, the $Case\,C$ configuration has poor accuracy like mono-models $ED1$ and $ED2$. Finally, $Case\,A$ model presents a good compromise between the other two multi-theory cases.

- The in-plane stress σ_{xx} is not sensitive to variable-kinematic modeling, except for the $Case\,A$ configuration where the transition elements are acting at the evaluation position, see Fig. 23.

By the evaluation of the various node-variable kinematic models, it is clear that an accurate representation of the stresses in localized zones is possible with DOFs reduction if an accurate distribution of the higher-order kinematic capabilities is performed. On the contrary, the accuracy of the solution in terms of displacements values depends on the global approximation over the whole structure. The efficacy of the DOFs reduction in variable-kinematics and global/local models, thus, depends on the characteristics of the problem under consideration as well as on the required analysis type.
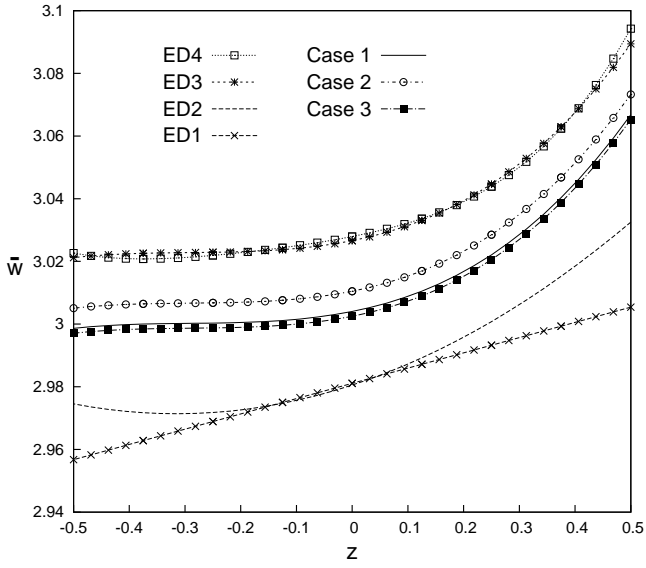
Figure 21: Transverse displacement $w(x; y) = w(a; b/2)$. Eight-layer composite plate.
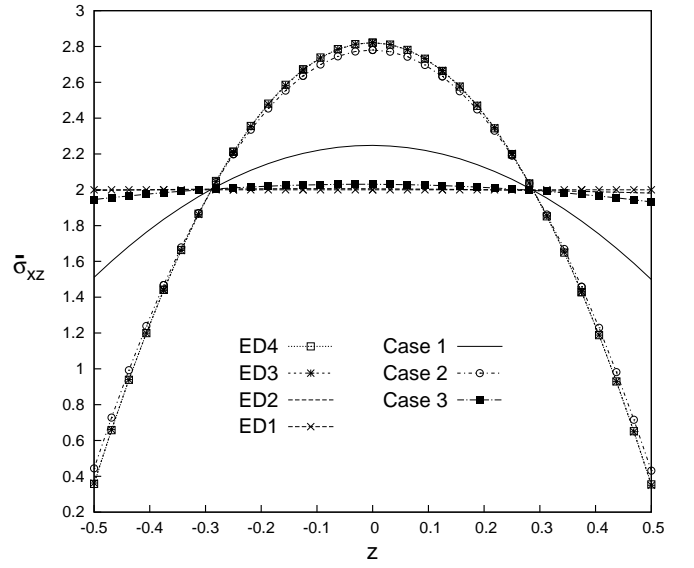

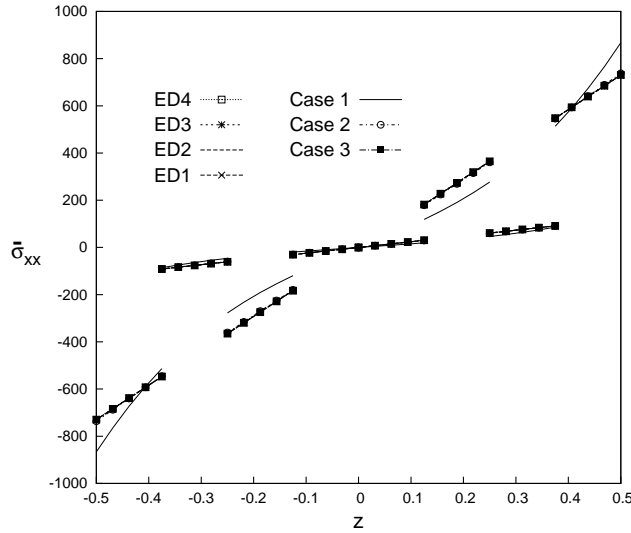Figure 22: Transverse shear stress $\sigma_{xz}(x; y) = \sigma_{xz}(a/2; b/2)$. Eight-layer composite plate.

Figure 23: In-plane stress $\sigma_{xx}(x; y) = \sigma_{xx}(a/2; b/2)$. Eight-layer composite plate.

4.3 Simply-supported cross-ply composite plates

A simply-supported composite plate is analysed as the final example. The geometrical dimensions are: $a = b = 0.1\,m$, the side-thickness ratio is $a/h = 10$. Symmetric $[0°/90°/0°]$ and anti-symmetric $[90°/0°]_2$ stacking sequences are considered. The material employed is orthotropic with he following properties: $E_L = 132.5\,GPa$, $E_T = 10.8\,GPa$, $G_{LT} = 5.7\,GPa$, $G_{TT} = 3.4\,GPa$, $\nu_{LT} = 0.24$, $\nu_{TT} = 0.49$. The plate is simply-supported and a localised uniform transverse pressure, $P = 1\,MPa$, is applied at top face on a square region of side length equal to $a/5 \times b/5$ and centered at the point $(a/2, b/2)$, see Fig. 24.

22

A convergence study versus the FE element size, i.e. the number of elements, is performed for the models considered in this paper and the $[0°/90°/0°]$ lamination is considered. In order to compare the results with other solutions present in literature [34], the mid-plane domain of the plane structure was subdivided into five zones along the axes x and z and they are shown in Fig. 24. The results from the convergence analysis are shown in Table. 5 and they are given in terms of transverse displacement w and in-plane normal stresses σ_{xx}, σ_{yy} evaluated at $(a/2, b/2, -h/2)$, and transverse shear stress σ_{xz} evaluated at $(5a/12, b/2, 0)$. As it is clear from this preliminary analysis, a non-uniform mesh grid of 20×20 elements ensures the convergence of the solution.
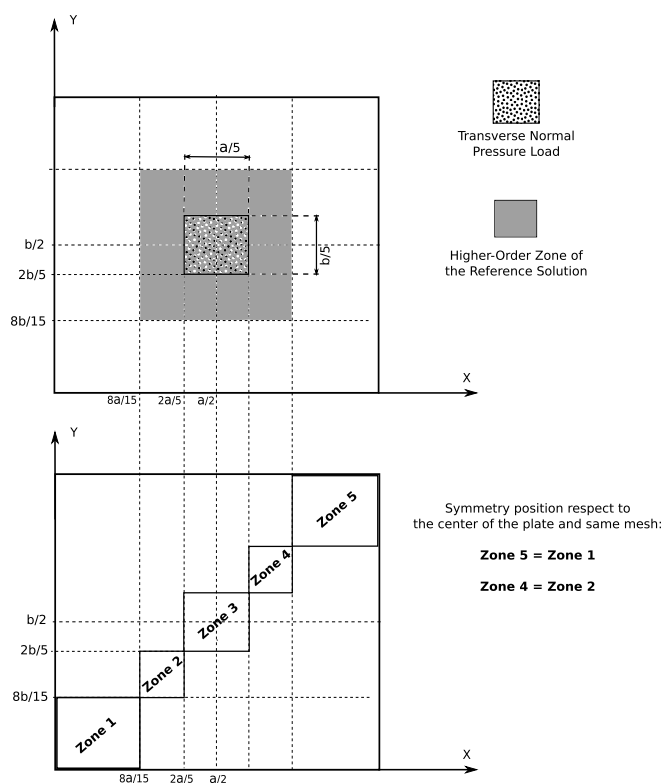

Figure 24: Cross-ply laminate subjected to localized pressure load and related FE mesh discretization into 5 zones.

Table 5: Convergence study with a $ED4$ plate element. Composite cross-ply symmetric plate with $(0°/90°/0°)$ lamination.

			$(-10^5)\,w$	σ_{xx}	σ_{yy}	$(-10)\,\sigma_{xz}$	$DOFs$
$Mesh\,10\times10$			1.661	12.493	2.187	5.977	6615
$zone1$	$zone2$	$zone3$					
2×2	2×2	2×2					
$Mesh\,16\times16$			1.660	12.057	2.025	5.754	16335
$zone1$	$zone2$	$zone3$					
3×3	3×3	4×4					
$Mesh\,20\times20$			1.660	12.058	2.026	5.756	25215
$zone1$	$zone2$	$zone3$					
4×4	4×4	4×4					
$Mesh\,12\times12$			1.660	12.054	2.024	5.744	9375
$zone1$	$zone2$	$zone3$					
2×2	2×2	4×4					
$Mesh\,16\times16$			1.660	11.972	2.012	5.853	16335
$zone1$	$zone2$	$zone3$					
2×2	2×2	8×8					
$Mesh\,20\times20$			1.660	11.956	2.008	5.847	25215
$zone1$	$zone2$	$zone3$					
2×2	2×2	12×12					

For the three-layer plate structure with $[0°/90°/0°]$ stacking sequence, mono-theory models are compared with those from the present global/local approach in Table 6. The table shows that mono-theory models with lower expansion order, $ED1$ and $ED2$, are not able to describe appropriately the transverse displacements w and the in-plane stresses σ_{xx} and σ_{yy}. To accurately describe the shear transverse stresses σ_{xz}, higher-order theories are required. Table 6 also show solutions from various node-variable kinematic CUF models with global/local capabilities used to perform the analysis of the proposed plate structure, and they are depicted in Fig. 25, where the mesh grid of a quarter of the plate is analysed. The two cases named as $Case\,A$ and $Case\,B$ are equivalent to the models $(ED1-ED4)^A$ and $(ED3-ED4)^B$ taken from [34] and in which, via the Arlequin method and 4-node Lagrangian plate elements, a fourth-order plate theory is used in correspondence of the loading and a first- and third-order kinematics is used outside the loading zone, respectively.

Table 6: Composite plate with $[0°/90°/0°]$ lamination. Transverse displacement $w = w(a/2, b/2, -h/2)$, in-plane normal stresses $\sigma_{xx} = \sigma_{xx}(a/2, b/2, -h/2)$ and $\sigma_{yy} = \sigma_{yy}(a/2, b/2, -h/2)$, and transverse shear stress $\sigma_{xz} = \sigma_{xz}(5a/12, b/2, 0)$ by various single- and multi-theory models.

	$(-10^5)\, w$	σ_{xx}	σ_{yy}	$(-10)\, \sigma_{xz}$	$DOFs^*$
Reference solutions [34]					
$3D$	1.674	11.94	2.019	6.524	
$LD4_a$	1.675	11.94	2.020	6.523	39
$LD4$	1.672	11.83	1.983	6.464	9984
$ED4_a$	1.660	11.95	2.005	5.865	15
$ED4$	1.657	11.85	1.985	5.830	3840
$(ED1 - ED4)^A$	1.609	11.92	1.962	5.848	2448
$(ED3 - ED4)^B$	1.657	11.84	1.985	5.831	3936
Present single- and multi-theory models					
$ED4$	1.660	11.96	2.008	5.847	6615
$ED3$	1.659	11.99	2.116	6.015	5292
$ED2$	1.562	10.19	1.794	3.852	3969
$ED1$	1.495	10.29	2.100	3.755	2646
$Case\,A$	1.604	12.01	1.982	5.851	5247
$Case\,B$	1.660	11.96	2.008	5.847	6159
$Case\,C$	1.526	11.73	1.945	4.941	4167
$Case\,D$	1.577	11.81	1.951	4.997	4983
$Case\,E$	1.566	11.79	1.946	5.004	4527
$Case\,F$	1.604	12.01	1.981	5.852	4887

$*$: for a fair comparison with reference solutions, DOFs are given for
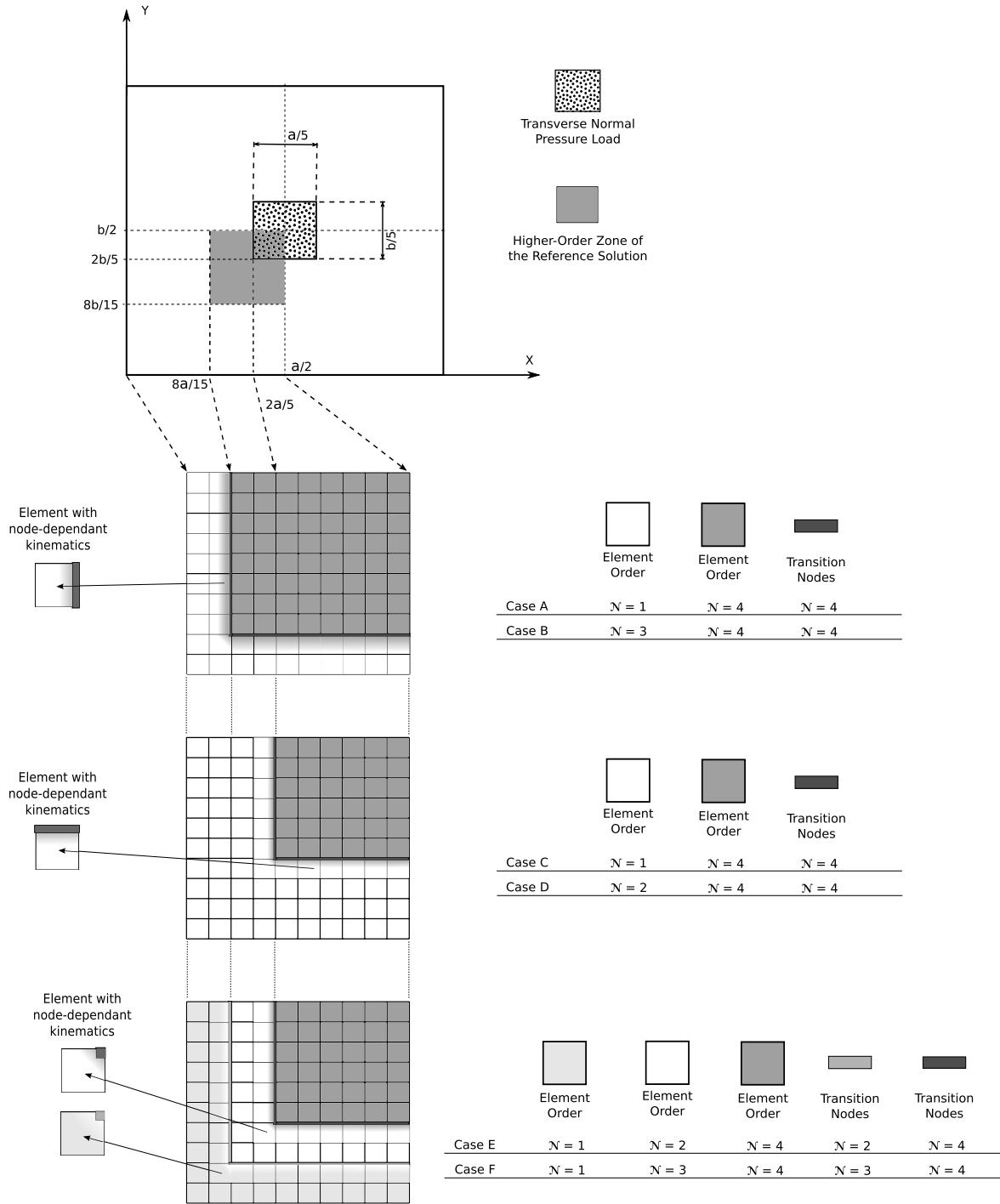one quarter of the plate structure

Y

a/5

Transverse Normal
Pressure Load

b/2

2b/5

b/5

8b/15

Higher-Order Zone of
the Reference Solution

X

8a/15

a/2

2a/5

Element with
node-dependant
kinematics

	Element Order	Element Order	Transition Nodes
Case A	$N = 1$	$N = 4$	$N = 4$
Case B	$N = 3$	$N = 4$	$N = 4$

Element with
node-dependant
kinematics

	Element Order	Element Order	Transition Nodes
Case C	$N = 1$	$N = 4$	$N = 4$
Case D	$N = 2$	$N = 4$	$N = 4$

Element with
node-dependant
kinematics

	Element Order	Element Order	Element Order	Transition Nodes	Transition Nodes
Case E	$N = 1$	$N = 2$	$N = 4$	$N = 2$	$N = 4$
Case F	$N = 1$	$N = 3$	$N = 4$	$N = 3$	$N = 4$

Figure 25: Graphical representation of the multi-theory models of the cross-ply plate structure.

Some results in terms of transverse displacement w, in-plane stress σ_{xx} and transverse shear stress σ_{xz} along the thickness are represented in Figs. 26, 27, and 28. The following remarks can be made:

- The transverse displacement w behaviour can change sensitively depending on the distribution of the kinematic enrichment within the structure plane. Table 6 and Fig. 26 show that $Case\,B$ has the same accuracy as the full higher-order $ED4$ model with a 8% DOFs reduction. Moreover, $Case\,F$ configuration has the same accuracy as $Case\,A$ with a 7% DOFs reduction. On the other

26

hand, $Case\,D$ is not so accurate, even though it makes use of the same number of DOFs as $Case\,F$.

- All the model proposed provide good approximation as far as the in-plane stresses distributions are concerned, see Fig. 27.

- For the evaluation of the transverse shear stress σ_{xz}, higher-order models are necessary in the regions close to loading zone. In fact, configurations $Case\,A$ and $Case\,B$ have the same behaviour as the mono-model theory $ED4$, meanwhile the other variable-kinematics configurations have a loss in accuracy, see Fig. 28.
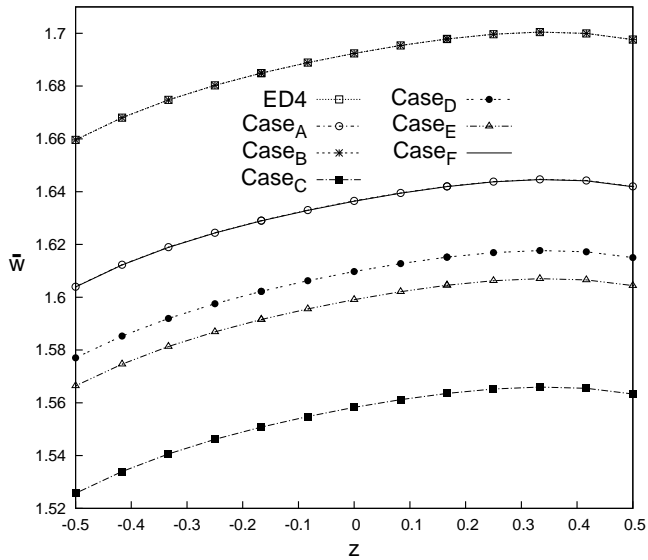
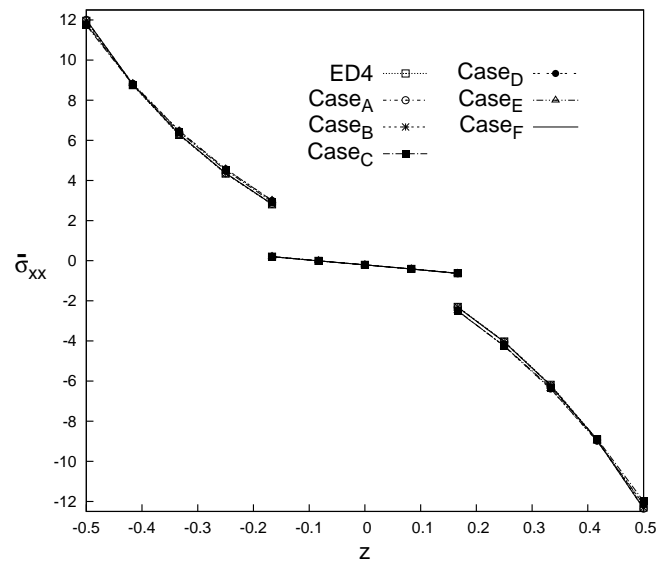Figure 26: Transverse displacement $w(x;y) = w(a/2;b/2)$. Composite 3 layered plate.

Figure 27: In-plane stress $\sigma_{xx}(x;y) = \sigma_{xx}(a/2;b/2)$. Composite 3 layered plate.
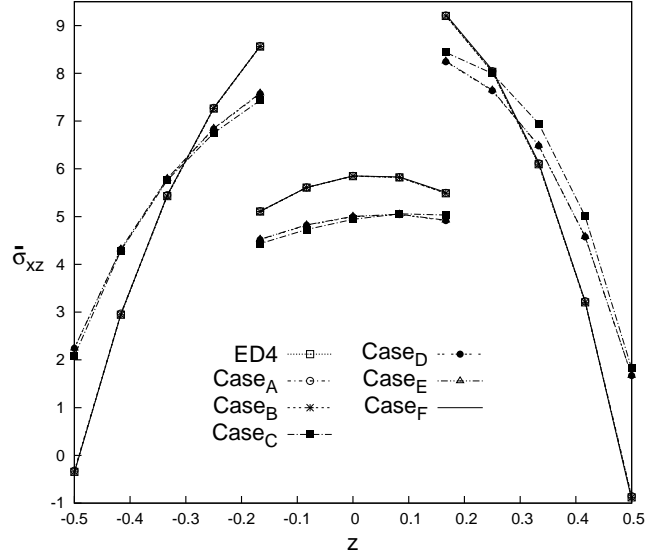
Figure 28: Transverse shear stress $\sigma_{xz}(x; y) = \sigma_{xz}(5a/12; b/2)$. Composite 3 layered plate.

Results in terms of transverse shear stress σ_{xz} and transverse normal stress σ_{zz} along the in-plane x axis are represented in Figs. 29 and 30, respectively. It has to be noticed that for the transverse shear stress σ_{xz} the $Case\,A$ and $Case\,C$ models are able to represent an accurate solution only in the loading zone, but for the major part of the plate length there is a 47% error with respect to $Case\,B$ model and mono-theory model $ED4$. For transverse normal stress σ_{zz}, all the modelling configurations lead to accurate results which are close to the mono-model $ED4$ solution.
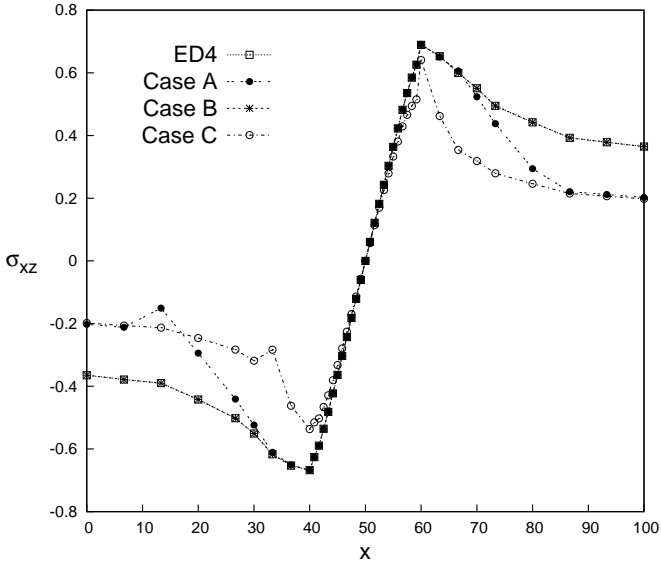

Figure 29: Transverse shear stress $\sigma_{xz}(y; z) = \sigma_{xz}(b/2; 0)$ along the plate axis x. Composite 3 layered plate.
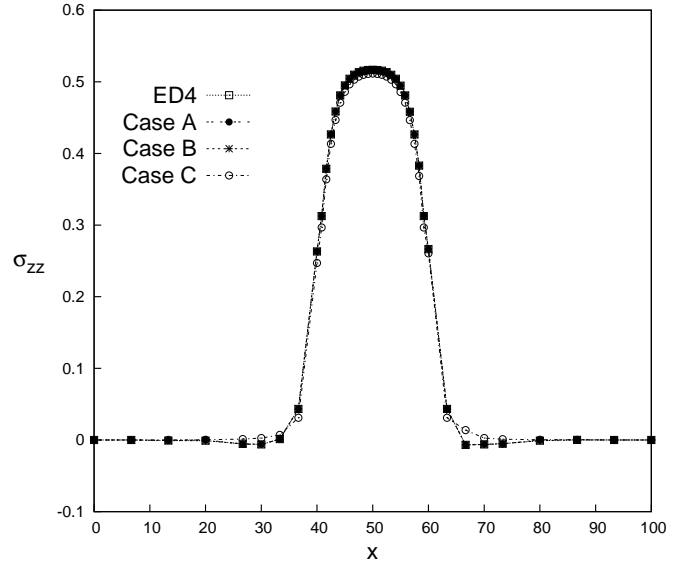

Figure 30: Transverse normal stress $\sigma_{zz}(y; z) = \sigma_{zz}(b/2; 0)$ along the plate axis x. Composite 3 layered plate.

Figures 31 and 32 show the three-dimensional distributions of the transverse shear stress σ_{xz} and transverse normal stress σ_{zz} from the mono-theory model $ED4$ and the variable-kinematic $Case\,A$

28

configuration. Again, the results show the enhanced global/local capabilities of the $CaseA$ model, which is able to predict correctly the stress state in the loading zone.
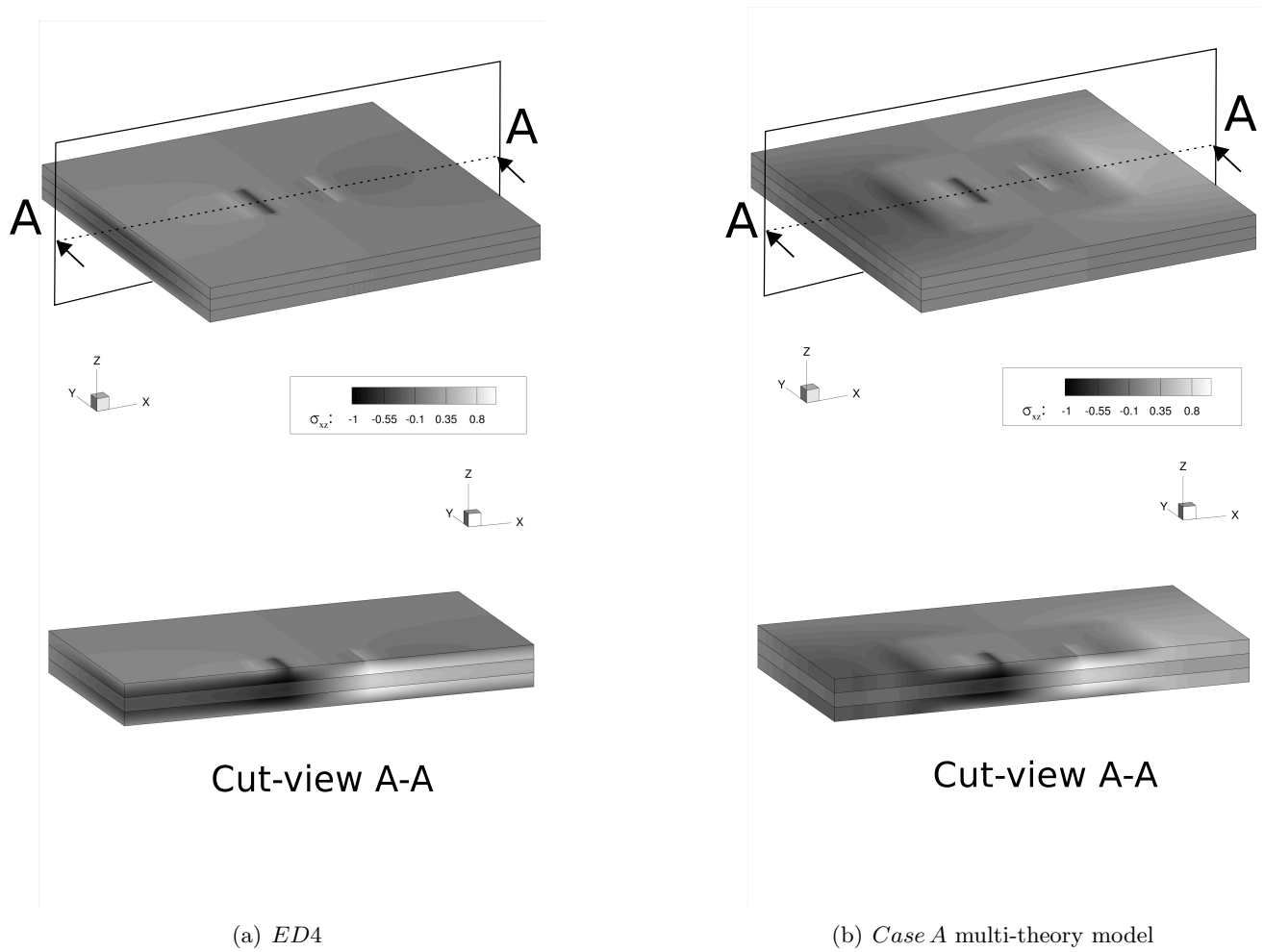

Cut-view A-A

Cut-view A-A

(a) $ED4$

(b) $Case\,A$ multi-theory model

Figure 31: Transverse shear stress σ_{xz}. Composite 3 layered plate.
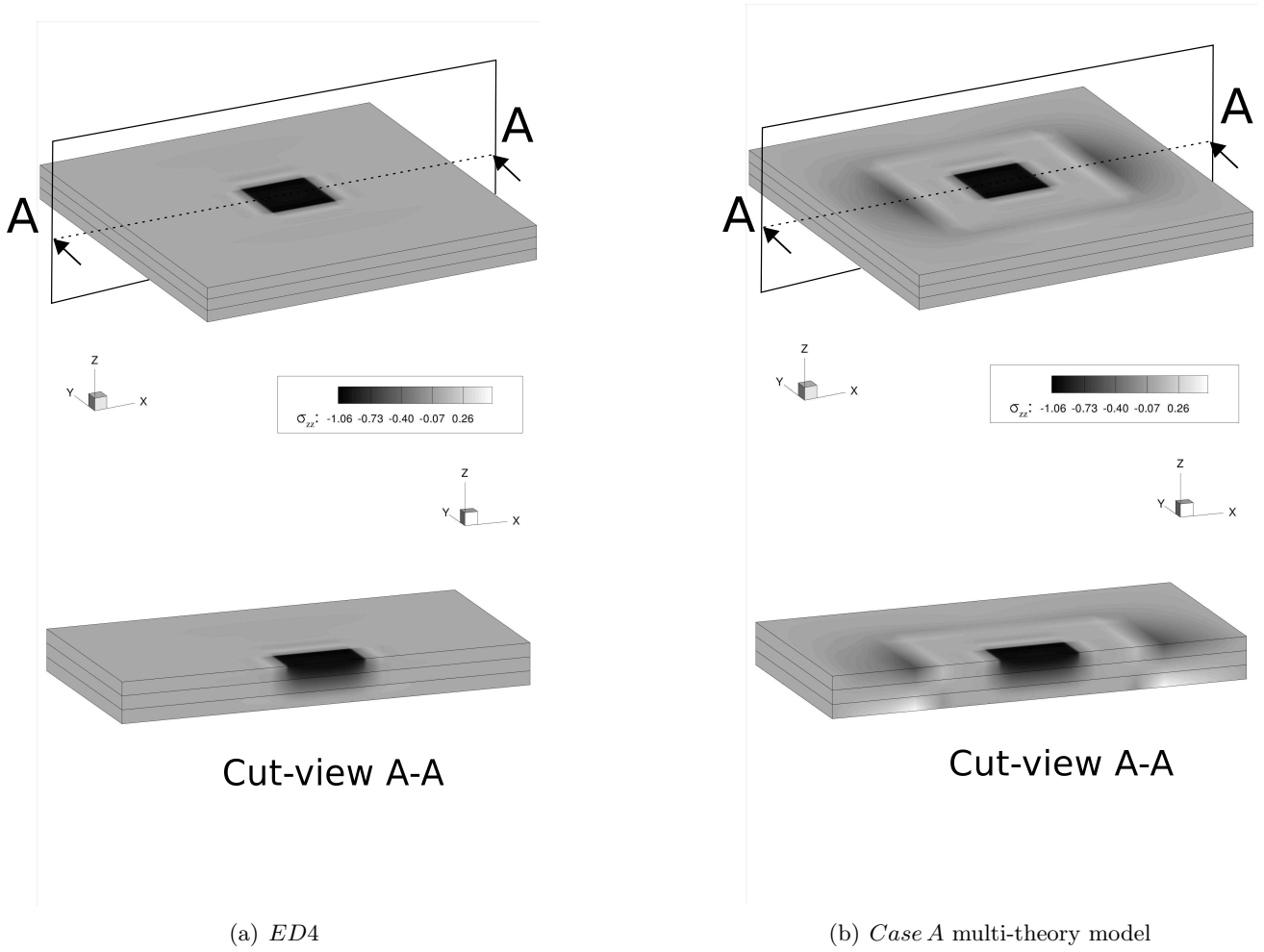
(a) *ED4*

(b) *Case A* multi-theory model

Figure 32: Transverse normal stress σ_{zz}. Composite 3 layered plate.

The anti-symmetric $[90°/0°]_2$ plate structure is finally considered, and some results are listed in Table 7. As in the previous analysis case, mono-model theories with lower expansion orders are not able to characterize the transverse displacements w and the in-plane stresses σ_{xx} and σ_{yy}. The description of the shear transverse stresses σ_{xz} at the interface between the second and third layers is not accurate in the case of ESL models, despite the approximation order. In fact, a layer-wise approximation is needed in this case to capture the complex three-dimensional behavior of the stress state. Nevertheless, Table 7 also shows the solutions from various node-variable kinematic CUF models, and they are the same as in the previous analysis case of the three-layer structures. Analogously as made in Table 6, even in this case the solutions from the present approach are successfully compared with those from [34], where the Arlequin method was used for global/local analysis.

Table 7: Composite plate with $[90°/0°/90°/0°]$ lamination. Transverse displacement $w = w(a/2, b/2, -h/2)$, in-plane normal stresses $\sigma_{xx} = \sigma_{xx}(a/2, b/2, -h/2)$ and $\sigma_{yy} = \sigma_{yy}(a/2, b/2, -h/2)$, and transverse shear stress $\sigma_{xz}^{L2/L3} = \sigma_{xz}(5a/12, b/2, 0^{+/-})$ by various single- and multi-theory models.

	$(-10^5)\, w$	σ_{xx}	σ_{yy}	$(-10)\,\sigma_{xz}^{L2}$	$(-10)\,\sigma_{xz}^{L3}$	$DOFs$
			Reference solutions [34]			
$3D$	1.719	11.28	1.823	6.104	6.104	
$LD4_a$	1.719	11.28	1.824	6.145	6.104	51
$LD4$	1.717	11.17	1.802	6.118	6.069	13056
$ED4_a$	1.700	11.28	1.789	8.267	4.931	15
$ED4$	1.698	11.19	1.778	8.214	4.899	3840
$(ED1 - ED4)^A$	1.746	10.95	1.750	8.262	4.928	2448
$(ED2 - ED4)^B$	1.668	11.20	1.778	8.259	4.926	3192
			Present single- and multi-theory models			
$ED4$	1.700	11.29	1.793	8.237	4.913	6615
$ED3$	1.677	10.99	1.914	8.439	5.034	5292
$ED2$	1.602	9.574	1.505	5.746	3.427	3969
$ED1$	1.525	9.966	1.712	5.680	3.388	2646
$Case\,A$	1.650	11.29	1.792	8.238	4.914	5247
$Case\,B$	1.668	11.31	1.794	8.239	4.914	6159
$Case\,C$	1.556	11.16	1.745	7.573	4.517	4167
$Case\,D$	1.622	11.19	1.758	7.567	4.514	4983
$Case\,E$	1.604	11.18	1.756	7.567	4.514	4527
$Case\,F$	1.640	11.29	1.777	8.185	4.883	4887

$*$: for a fair comparison with reference solutions, DOFs are given for
one quarter of the plate structure

The distributions of the transverse displacement w and the transverse shear stress σ_{xz} along the thickness are represented in Figs. 33 and 34. Moreover, three-dimensional representations of the stress state components σ_{xz} and σ_{zz} are shown in Figs. 35 and 36, where a multi-theory model is compared to the full $ED4$ model. All the results confirm the previous comments an the efficacy of the proposed formulation.
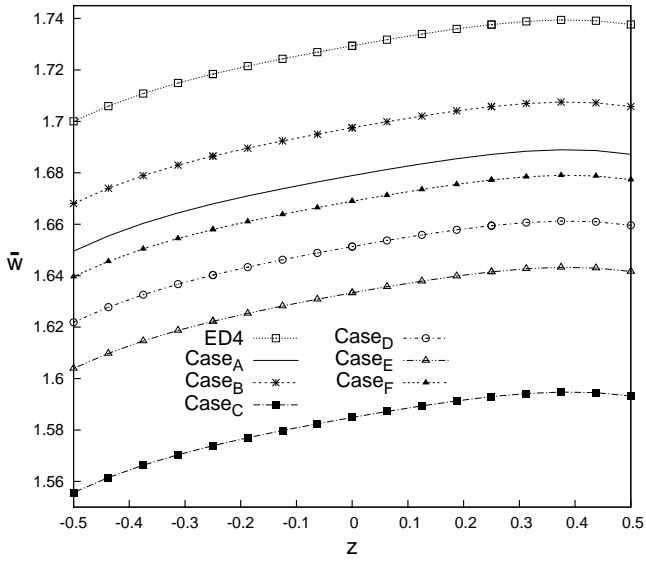
Figure 33: Transverse displacement $w(x; y) = w(a/2; b/2)$. Composite 4 layered plate.
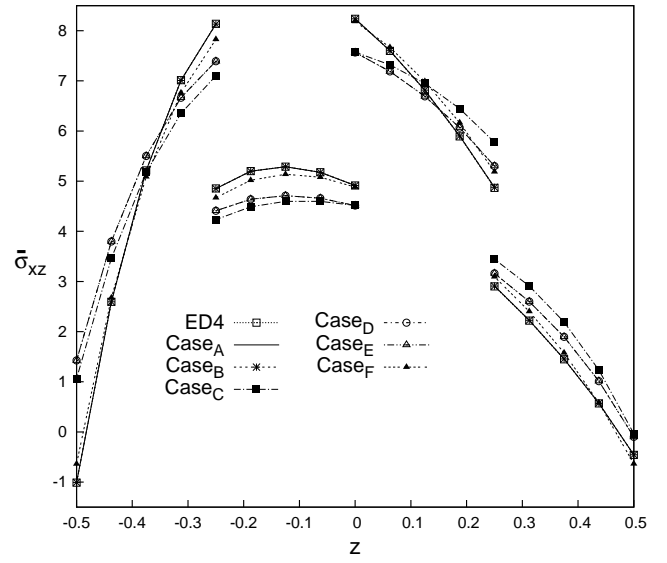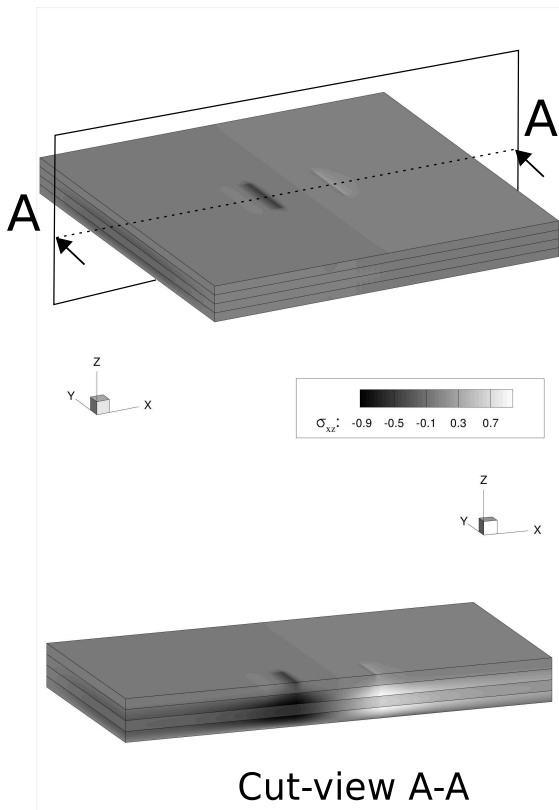

Figure 34: Transverse shear stress $\sigma_{xz}(x; y) = \sigma_{xz}(5a/12; b/2)$. Composite 4 layered plate.
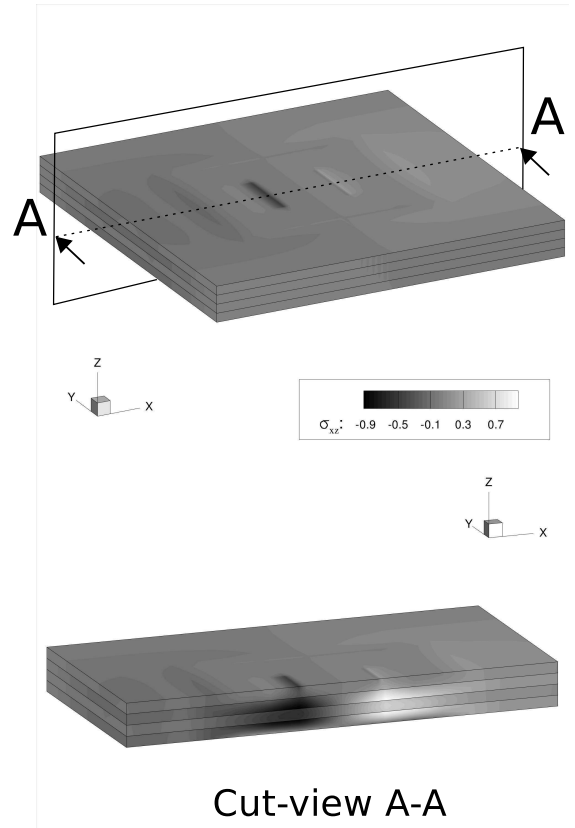
Cut-view A-A

Cut-view A-A

(a) *ED4*

(b) *Case A* multi-theory model

Figure 35: Transverse shear stress σ_{xz}. Composite 4 layered plate.
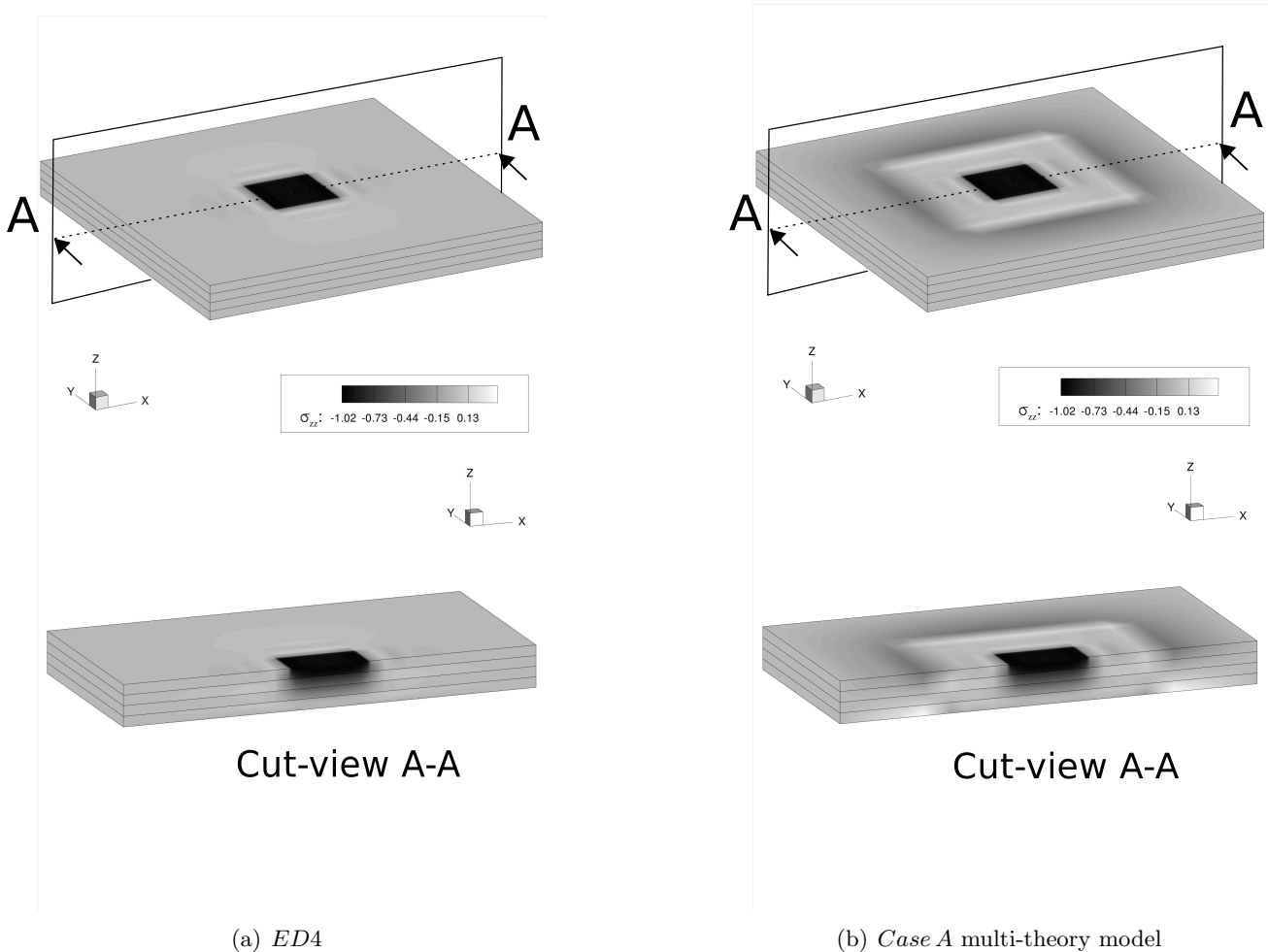
(a) *ED4*

(b) *Case A* multi-theory model

Figure 36: Transverse normal stress σ_{zz}. Composite 4 layered plate.

5 Conclusions

A new methodology for global/local analysis of metallic and composite plate structure has been introduced in this paper. This approach makes use of advanced finite plate elements with node-dependent kinematics, which are formulated in the domain of the Carrera Unified Formulation (CUF). By employing CUF, in fact, the finite element arrays of the generic plate element are formulated in terms of *fundamental nuclei*, which are invariants of the theory approximation order. In this manner, the plate theory can vary within the same finite elements with no difficulties. Thus, given a finite element model, the theory approximation accuracy can be enriched locally in a very straightforward manner by enforcing the same kinematics at the interface nodes between kinematically incompatible plate elements. The resulting global/local approach is very efficient because it does not employ any mathematical artifice to enforce the displacement/stress continuity, such as those methods based on Lagrange multipliers or overlapping regions. Thus, the stiffness matrix of the variable kinematics element preserves the important numerical properties of the usual finite element arrays, is definite positive, and is rank sufficient (i.e., it does not possess any zero-energy kinematic modes other than rigid body modes).

The proposed methodology has been widely assessed in this paper by analysing metallic and composite plates and by comparison with solutions from the literature and those from finite element commercial tools. Future developments will deal with the extension of this global/local methodology to hierarchical

shell theories and layer-wise methods.

References

[1] W T Koiter. On the foundations of the linear theory of thin elastic shell. *Proc. Kon. Nederl. Akad. Wetensch.*, 73:169–195, 1970.

[2] P G Ciarlet and L Gratie. Another approach to linear shell theory and a new proof of Korn's inequality on a surface. *C. R. Acad. Sci. Paris*, I,340:471–478, 2005.

[3] E Reissner and Y Stavsky. Bending and stretching of certain types of heterogeneous aelotropic elastic plates. *Journal of Applied Mechanics*, 28:402–408, 1961.

[4] E Reissner. The effect of transverse shear deformation on the bending of elastic plates. *Journal of Applied Mechanics*, 12(2):69–77, 1945.

[5] R D Mindlin. Influence of rotary inertia and shear flexural motion of isotropic, elastic plates. *Journal of Applied Mechanics*, 18:31–38, 1951.

[6] T Kant, D R J Owen, and O C Zienkiewicz. Refined higher order C^0 plate bending element. *Computer & Structures*, 15:177–183, 1982.

[7] T Kant and J R Kommineni. Large amplitude free vibration analysis of cross-ply composite and sandwich laminates with a refined theory and C^0 finite elements. *Computer & Structures*, 50:123–134, 1989.

[8] J N Reddy. Mechanics of laminated composite plates and shells. *Theory and Analysis, CRC Press*, 1997.

[9] A N Palazotto and S T Dennis. Nonlinear analysis of shell structures. *AIAA Series*, 1992.

[10] R E Bank. Adaptive computational methods for partial differential equations. *SIAM*, 1983.

[11] B A Szabo and I Babuska. Finite element analysis. *John Wiley & Sons*, 1991.

[12] K J Bathe. Finite element procedure. *Prentice Hall*, 1996.

[13] D M Thompson and O H Jr Griffin. 2-D to 3-D Global/Local Finite Element Analysis of Cross-Ply Composite Laminates. *Journal of Reinforced Plastics and Composites*, 9:492–502, 1990.

[14] K M Mao and C T Sun. A Refined Global-Local Finite Element Analysis Method. *International Journal for Numerical Methods in Engineering*, 32:29–43, 1991.

[15] J D Whitcomb and K Woo. Application of Iterative Global/Local Finite Element Analysis. Part 1: Linear Analysis. *Communications in Numerical Methods in Engineering*, 9(9):745–756, 1993.

[16] J D Whitcomb and K Woo. Application of Iterative Global/Local Finite Element Analysis. Part 2: Geometrically Non-Linear Analysis. *Communications in Numerical Methods in Engineering*, 9(9):757–766, 1993.

[17] A S D Wang and F W Crossman. Calculation of Edge Stresses in Multi-Layer by Sub-Structuring. *Journal of Composite Materials*, 12:76–83, 1978.

[18] N J Pagano and S R Soni. Global-Local Laminate Variational Model. *International Journal of Solids and Structures*, 19(3):207–228, 1983.

[19] R Jones, R Callinan, K K Teh, and K C Brown. Analysis of Multi-Layer Laminates Using Three-Dimensional Super Elements. *International Journal for Numerical Methods in Engineering*, 20(3):583–587, 1984.

[20] A Pagani, S Valvano, and E Carrera. Analysis of laminated composites and sandwich structures by variable-kinematic MITC9 plate elements. *Journal of Sandwich Structures and Materials*. In Press. DOI: 10.1177/1099636216650988.

[21] M Botshekanan Dehkordi, M Cinefra, S M R Khalili, and E Carrera. Mixed LW/ESL models for the analysis of sandwich plates with composite faces. *Composite Structures*, 98:330–339, 2013.

[22] M Botshekanan Dehkordi, S M R Khalili, and E Carrera. Non-linear transient dynamic analysis of sandwich plate with composite face-sheets embedded with shape memory alloy wires and flexible core- Based on the mixed LW (Layer-wise)/ESL (Equivalent single layer) models. *Composites Part B*, 87:59–74, 2016.

[23] F Brezzi and L D Marini. The three-field formulation for elasticity problems. *GAMM Mitteilungen*, 28:124–153, 2005.

[24] E Carrera, A Pagani, and M Petrolo. Use of Lagrange multipliers to combine 1D variable kinematic finite elements. *Computers and Structures*, 129:194–206, 2013.

[25] E. Carrera and A. Pagani. Analysis of reinforced and thin-walled structures by multi-line refined 1D/beam models. *International Journal of Mechanical Sciences*, 75:278–287, 2013.

[26] E. Carrera and A. Pagani. Multi-line enhanced beam model for the analysis of laminated composite structures. *Composites: Part B*, 57:112–119, 2014.

[27] H Ben Dhia. Multiscale mechanical problems: the Arlequin method. *Comptes Rendus de lAcademie des Sciences Series IIB Mechanics Physics Astronomy*, 326(12):899–904, 1998.

[28] H Ben Dhia. Numerical modelling of multiscale problems: the Arlequin method. *CD Proceedings of ECCM99, Munchen*, 1999.

[29] H Ben Dhia. Further insights by theoretical investigations of the multiscale Arlequin method. *International Journal for Multiscale Computational Engineering*, 6(3):215–232, 2008.

[30] H Ben Dhia. he Arlequin method as a flexible engineering tool. *International Journal for Numerical Methods in Engineering*, 62(11):1442–1462, 2005.

[31] H Hu, S Belouettar, M Potier-Ferry, and E M Daya. Multi-scale modelling of sandwich structures using the Arlequin method. Part I: linear modelling. *Finite Elements in Analysis and Design*, 45(1):37–51, 2008.

[32] H Hu, S Belouettar, M Potier-Ferry, E M Daya, and A Makradi. Multi-scale nonlinear modelling of sandwich structures using the Arlequin method. *Finite Elements in Analysis and Design*, 92(2):515–522, 2010.

[33] F Biscani, G Giunta, S Belouettar, E Carrera, and H Hu. Variable kinematic beam elements coupled via Arlequin method. *Composite Structures*, 93(2):697–708, 2011.

[34] F Biscani, G Giunta, S Belouettar, E Carrera, and H Hu. Variable kinematic plate elements coupled via Arlequin method. *International Journal for Numerical Methods in Engineering*, 91:1264–1290, 2012.

[35] J N Reddy and D H Robbins. Theories and computational models for composite laminates. *Applied Mechanics Review*, 47:147–165, 1994.

[36] Junuthula N Reddy. Mechanics of laminated composite plates- Theory and analysis(Book). *Boca Raton, FL: CRC Press, 1997.*, 1997.

[37] J Fish. The s-version of the finite element method. *Computers and Structures*, 43(3):539–547, 1992.

[38] J Fish and S Markolefas. Adaptive s-method for linear elastostatics. *Computer Methods in Applied Mechanics and Engineering*, 103:363–396, 1993.

[39] C Wenzel, P Vidal, M D'Ottavio, and O Polit. Coupling of heterogeneous kinematics and Finite Element approximations applied to composite beam structures. *Composite Structures*, 116:177–192, 2014.

[40] E Carrera and E Zappino. Analysis of complex structures coupling variable kinematics one-dimensional models. In *ASME 2014 International Mechanical Engineering Congress and Exposition*, Montreal, Quebec, Canada, November 2014.

[41] E Carrera. Theories and finite elements for multilayered, anisotropic, composite plates and shells. *Archives of Computational Methods in Engineering*, 9(2):87–140, 2002.

[42] E Carrera. Theories and finite elements for multilayered plates and shells: a unified compact formulation with numerical assessment and benchmarking. *Archives of Computational Methods in Engineering*, 10(3):215–296, 2003.

[43] K J Bathe and E Dvorkin. A formulation of general shell elements - the use of mixed interpolation of tensorial components. *International Journal for Numerical Methods in Engineering*, 22:697–722, 1986.

[44] K J Bathe and F Brezzi. A simplified analysis of two plate bending elements-the MITC4 and MITC9 elements. *Proceedings, Numerical Methods in Engineering: Theory and Applications*, 1987.

[45] K J Bathe, F Brezzi, and S W Cho. The MICT7 and MITC9 plate bending elements. *Computers & Structures*, 32(3-4):797–814, 1989.

[46] M L Bucalem and E Dvorkin. Higher-order MITC general shell elements. *International Journal for Numerical Methods in Engineering*, 36:3729–3754, 1993.

[47] E Carrera, M Cinefra, and E Petrolo M. abd Zappino. *Finite Element Analysis of Structures through Unified Formulation*. John Wiley & Sons, 2014.

[48] E Carrera. Multilayered shell theories accounting for layerwise mixed description, Part 1: governing equations. *AIAA Journal*, 37(9):1107–1116, 1999.

[49] E Carrera. Multilayered shell theories accounting for layerwise mixed description, Part 2: numerical evaluations. *AIAA Journal*, 37(9):1117–1124, 1999.

[50] M Cinefra, S Valvano, and E Carrera. Heat conduction and Thermal Stress Analysis of laminated composites by a variable kinematic MITC9 shell element. *Curved and Layered Structures*, 1:301–320, 2015.

[51] M Cinefra, S Valvano, and E Carrera. Thermal Stress Analysis of laminated structures by a variable kinematic MITC9 shell element. *Journal of Thermal Stresses*, 39(2):121–141, 2016.

[52] Maria Cinefra, Erasmo Carrera, and Stefano Valvano. Variable Kinematic Shell Elements for the Analysis of Electro-Mechanical Problems. *Mechanics of Advanced Materials and Structures*, 22(1-2):77–106, September 2015.

[53] M Cinefra, S Valvano, and E Carrera. A layer-wise MITC9 finite element for the free-vibration analysis of plates with piezo-patches. *International Journal of Smart and Nano Materials*, 6(2):85–104, 2015.

[54] E. Carrera. Historical review of Zig-Zag theories for multilayered plates and shells. *Applied Mechanics Reviews*, 56:287–308, 2003.

[55] E. Carrera. On the use of the Murakami's zig-zag function in the modeling of layered plates and shells. *Computers and Structures*, 82:541–554, 2004.

[56] E. Carrera. Mixed layer-wise models for multilayered plates analysis. *Composite Structures*, 43:57–70, 1998.

[57] E. Carrera. Evaluation of Layerwise Mixed Theories for Laminated Plates Analysis. *Applied Mechanics Reviews*, 36(5):830–839, 1998.

[58] M. Cinefra and S. Valvano. A variable kinematic doubly-curved MITC9 shell element for the analysis of laminated composites. *Mechanics of Advanced Materials and Structures*, 23(11):1312–1325, 2016.

[59] J N Reddy. An evaluation of equivalent-single-layer and layerwise theories of composite laminates. *Composite Structures*, 25:21–35, 1993.

[60] S G Lekhnitskii. Anisotropic Plates. In *Tsai, S W and Cheron, T editors (Translated from 2nd Russian Edition)*. Gordon & Branch, 1968.

[61] S H Nguyen and K S Surana. Two-dimensional curved beam element with higher-order hierarchical transverse approximation for laminated composites. *Computers & Structures*, 36:499–511, 1990.

[62] J F Davalos, Kim Y, and Barbero E J. Analysis of laminated beams with a layerwise constant shear theory. *Computers & Structures*, 28:241–253, 1994.

[63] Y Z Xiaoshan Lin. A novel one-dimensional two-node shear-flexible layered composite beam element. *Finite Elements in Analysis and Design*, 47:676–682, 2011.

[64] T P Vo and H T Thai. Static behavior of composite beams using various refined shear deformation theories. *Computers & Structures*, 94:2513–2522, 2012.